

Potential Induced Degradation (PID) of Pre-Stressed Photovoltaic Modules:  
Effect of Glass Surface Conductivity Disruption

by

Sai Ravi Vasista Tatapudi

A Thesis Presented in Partial Fulfillment  
of the Requirements for the Degree  
Master of Science in Technology

Approved November 2012 by the  
Graduate Supervisory Committee:

Govindasamy Tamizhmani, Chair  
Devarajan Srinivasan, Member  
Bradley Rogers, Member

ARIZONA STATE UNIVERSITY

December 2012

## ABSTRACT

Potential induced degradation (PID) due to high system voltages is one of the major degradation mechanisms in photovoltaic (PV) modules, adversely affecting their performance due to the combined effects of the following factors: system voltage, superstrate/glass surface conductivity, encapsulant conductivity, silicon nitride anti-reflection coating property and interface property (glass/encapsulant; encapsulant/cell; encapsulant/backsheet). Previous studies carried out at ASU's Photovoltaic Reliability Laboratory (ASU-PRL) showed that only negative voltage bias (positive grounded systems) adversely affects the performance of commonly available crystalline silicon modules. In previous studies, the surface conductivity of the glass surface was obtained using either conductive carbon layer extending from the glass surface to the frame or humidity inside an environmental chamber. This thesis investigates the influence of glass surface conductivity disruption on PV modules. In this study, conductive carbon was applied only on the module's glass surface without extending to the frame and the surface conductivity was disrupted (no carbon layer) at 2cm distance from the periphery of frame inner edges. This study was carried out under dry heat at two different temperatures (60 °C and 85 °C) and three different negative bias voltages (-300V, -400V, and -600V). To replicate closeness to the field conditions, half of the selected modules were pre-stressed under damp heat for 1000 hours (DH 1000) and the remaining half under 200 hours of thermal cycling (TC 200). When the surface continuity was disrupted by maintaining a 2 cm gap

from the frame to the edge of the conductive layer, as demonstrated in this study, the degradation was found to be absent or negligibly small even after 35 hours of negative bias at elevated temperatures. This preliminary study appears to indicate that the modules could become immune to PID losses if the continuity of the glass surface conductivity is disrupted at the inside boundary of the frame. The surface conductivity of the glass, due to water layer formation in a humid condition, close to the frame could be disrupted just by applying a water repelling (hydrophobic) but high transmittance surface coating (such as Teflon) or modifying the frame/glass edges with water repellent properties.

## ACKNOWLEDGMENTS

I would like to thank Dr. Govindasamy TamizhMani for encouraging me to work on this topic and guiding me through it. I would like to thank Dr. Bradley Rogers and Dr. Devarajan Srinivasan for being my part of my advising committee. I would also like to thank Dr. Joseph Kuitche, lab manager of ASU-PRL for his support throughout the project. I would like to thank Mrs. Sandhya Goranti and Mr. Faraz Ebneali for helping me with the initial experimental setup. I would also like to thank the following current and former ASU-PRL students for their help: Mr. Kartheek Koka, Mr. Jose Cano, Ms. Meenagupta Vemula, Ms. Quratul Ain Shah, Mr. Kolapo Olakonu, Mr. Surayanarayana Vasanthajanakiraman, Mr. Brett Knisely and Mr. Saurabh Chatterjee. Finally, I would like to thank my parents, my sister and brother-in-law for their continued support.

## TABLE OF CONTENTS

	Page
LIST OF TABLES .....	vi
LIST OF FIGURES .....	ix
CHAPTER	
1. INTRODUCTION.....	1
1.1 Background .....	1
1.2 Statement of purpose .....	4
1.3 Scope .....	5
2. LITERATURE REVIEW .....	9
2.1 Reliability and acceleration testing .....	10
2.2 Types of Acceleration Tests.....	12
2.3 Types of Conductivity .....	14
2.4 Potential Induced Degradation (PID).....	15
3. METHODOLOGY .....	21
3.1 Characterization .....	23
3.1.1 Visual Inspection.....	23
3.1.2 Electro-luminescence (EL) Image Inspection.....	24
3.1.4 Performance Comparison.....	28
3.2 PID Stress.....	32
3.2.1 Equipment/Material Used .....	32
3.2.2 Procedure .....	35
4. RESULTS AND DISCUSSION.....	42
4.1 Partial Carbon.....	38

CHAPTER	Page
4.2 Full Carbon .....	43
4.4 Determination of Activation Energy .....	49
4.5 Charge Transferred.....	51
4.6 Potential Induced Recovery .....	52
4.7 Calculation of Series Resistance ( $R_S$ ).....	54
4.7 Image Characterization.....	56
4.8 Summary of PID Evaluations at ASU-PRL.....	58
5. DISCUSSION .....	65
REFERENCES.....	67
APPENDIX	
A.....	70
B.....	73
C.....	76
D.....	78
E.....	81
F.....	84
G.....	91

## LIST OF TABLES

Table	Page
2.1. Relation between failure mechanism, field failure symptom and acceleration test . . . . .	12
3.1. Table describing the project parameters. . . . .	39
4.1. Performance comparison after PID under partial carbon condition at 60 °C. . . . .	42
4.2. Performance comparison after PID under partial carbon condition at 85 °C. . . . .	45
4.3. Performance comparison after PID under full carbon condition at 60 °C. ....	44
4.4. Performance comparison after PID under full carbon condition at 85 °C. ....	45
4.7. Activation energies of modules stressed at -300 V and 85 °C. ....	51
4.8. Coulombs transferred. ....	52
4.9. Test parameters during recovery for Mfg7 under full carbon condition. ....	52
4.10. Power recovered after recovery test for manufacturer 7. ....	53
4.11. Series resistance values for MFG 7 modules. ....	56
4.12. Electro-luminescence images of a TC1 module (mfg5). ....	57
4.13. Infrared images of a DH1 module (mfg6). ....	58
A 1. Performance measurement of manufacturer 5 during PID testing. ....	72
A 2. Performance measurement of manufacturer 6 during PID testing under partial carbon condition . . . . .	72

Table	Page
A 3. Performance measurement of manufacturer 7 during 35 Hrs. of partial carbon PID testing.....	73
A 4. Performance measurement of manufacturer 7 during 35 Hrs. of full carbon PID testing.....	73
B 1. Comparison of performance of Mfg 5 modules before and after recovery...	75
B 2. Comparison of performance of Mfg 6 modules before and after recovery...	74
B 3. Comparison of performance of Mfg 7 modules before and after recovery...	75
F 1. EL images of the MFG5 DH1 module through various test stages.....	85
F 2. EL images of the MFG5 TC1 module through various test stages. ....	85
F 3. EL images of the MFG5 DH2 module through various test stages.....	86
F 4. EL images of the MFG5 TC2 module through various test stages. ....	86
F 5. EL images of the MFG6 DH1 module through various test stages.....	87
F 6. EL images of the MFG6 TC1 module through various test stages. ....	87
F 7. EL images of the MFG6 DH2 module through various test stages.....	88
F 8. EL images of the MFG6 TC2 module through various test stages. ....	88
F 9. EL images of the MFG7 DH1 module through various test stages.....	89
F 10. EL images of the MFG7 TC1 module through various test stages. ....	89
F 11. EL images of the MFG7 DH2 module through various test stages.....	90
F 12. EL images of the MFG7 TC2 module through various test stages. ....	90
G 1. IR images of MFG5 DH1 module through various test stages.....	93
G 2. IR images of MFG5 TC1 module through various test stages. ....	93



Table	Page
G 3. IR images of MFG5 DH2 module through various test stages.....	93
G 4. IR images of MFG5 TC2 module through various test stages. ....	93
G 5. IR images of MFG6 DH1 module through various test stages.....	94
G 6. IR images of MFG6 TC1 module through various test stages. ....	94
G 7. IR images of MFG6 TC2 module through various test stages. ....	95
G 8. IR images of MFG6 DH2 module through various test stages.....	95
G 9. IR images of MFG7 DH1 module through various test stages.....	96
G 10. IR images of MFG7 TC1 module through various test stages. ....	96
G 11. IR images of MFG7 DH2 module through various test stages.....	97
G 12. IR images of MFG7 TC2 module through various test stages. ....	97

## LIST OF FIGURES

Figure	Page
1.1. A Bath tub curve depicting failure rates at various periods in a products lifetime.....	2
1.2. Voltage & polarity depending upon its position and grounding .....	3
1.3A. High Surface Conductivity (full surface carbon) .....	7
1.3B. Low Surface Conductivity.....	7
1.3C. Disrupted Surface Conductivity.....	7
2.1. Equivalent circuit of a PV cell.....	10
2.2. Temperature (°C) Vs. Time (h) for a thermal cycling stress test .....	13
2.3. Leakage current pathways in a PV module .....	15
2.4. Influence of full surface conductivity (carbon or humidity) of glass on PID at +600 V .....	18
2.5. Influence of full surface conductivity (carbon or humidity) of glass on PID at -600 V .....	19
2.6. String circuit diagram for an array at APS-STAR facility.....	20
2.7. Influence of PID on 1,155 modules with respect to module position in the string.....	21
3.1. Overall methodology followed during PID stress testing.....	22
3.2. Flow chart.....	23
3.3. Characterization of modules.....	24
3.4. Visual inspection was performed under natural sunlight.....	25

Figure	Page
3.5. An EL camera, a power supply and a computer are used to capture EL images.....	26
3.6. A module is shown on an adjustable rack in front of the EL camera. ....	26
3.7. A module is shown to be placed securely on the rack. ....	27
3.8. EL images are taken before, during and after PID and recovery. ....	28
3.9. An example of an IR image of a module along with temperature scale. ....	29
3.10. The effect of light on the current-voltage characteristics of a p-n junction. ....	30
3.11. Daystar DS 100 IV curve tracer (top-left), Reference cells (top-right), Sundial (bottom). ....	31
3.12. Performance measured using IVPC 3.05 software. ....	33
3.13. A Keithley 2700 data logger used in the experiments ....	34
3.14. Front side control panel of the PS350 power supply. ....	35
3.15. Circuit diagram of the PID box ....	36
3.16. Modules hanging from ceramic insulators on a rack. ....	37
3.17. Positive from the power supply is connected to the grounding point.....	38
4.1. Frame without carbon coating; Glass with carbon coating;.....	40
4.2. Performance comparison after PID under partial carbon condition at 60 °C for 70 hours. ....	43
4.3. Performance comparison after PID under partial carbon condition at 85 °C. ....	45
4.4. Frame with carbon coating; glass with carbon ....	45
4.5. Performance comparison after PID under full carbon condition at 60 °C. ....	47
4.6. Performance comparison after PID under full carbon condition at 85 °C. ....	48

Figure	Page
4.7. Performance degradation due to PID for all the modules. ....	50
4.8. Influence of continuity of glass surface conductivity on PID .....	51
4.9. Arrhenius plot for Mfg 5 during first 5 hours of PID stress.....	54
4.10. Performance comparison before and after potential induced recovery. ....	57
4.11. Calculating $R_s$ of TC1 MFG7 module after full carbon PID by single slope method.....	58
4.12. Calculating $R_s$ of TC1 MFG7 module after PIR by single slope method...	59
4.13. PV modules with no surface conductive layers.....	64
4.14. Surface conductivity of glass with full surface carbon (A), with humidity (B), with no water layer near the frame (C) and with no carbon layer near the frame (D) .....	65
4.15. +600V: Influence of module history, stress temperature or surface conductivity .....	66
C 1. Leakage current ( $\mu A$ ) versus time (Hrs.) for TC1 and DH1 (Mfg7) .....	77
C 2. Leakage current ( $\mu A$ ) versus time (Hrs.) for TC2 and DH2 (Mfg7) .....	77
D 1. Arrhenius plot for TC1 and DH1 (Mfg 5) during first stage (5 hours of PID). .....	79
D 2. Arrhenius plot for TC1 and DH1 (Mfg 5) during second stage (5 hours of PID). .....	79
D 3. Arrhenius plot for TC1 and DH1 (Mfg 5) during third stage (25 hours of PID). .....	80

Figure	Page
E 1. Pre and post-recovery dark IVs (log scale) comparison for MFG7 DH1 module. ....	82
E 2. Pre and post-recovery dark IVs (log scale) comparison for MFG5 DH2 module. ....	82
E 3. Pre and post-recovery dark IVs (log scale) comparison for MFG7 TC1 module. ....	83
E 4. Pre and post-recovery dark IVs (log scale) comparison for MFG7 TC2 module. ....	83

# CHAPTER 1

## INTRODUCTION

### 1.1 Background

As large scale deployment of photovoltaic (PV) modules is becoming a reality, the modules must withstand various field conditions to remain operative through their warranty periods. Increased array life and reliability directly influence the economic viability of PV as an energy source. After considering present-value discounting and escalation of the worth of electricity in future, a PV plant with a 30-year life expectancy is worth 25-30 % more than a plant with 20-year life expectancy [1]. Therefore, reliability of the modules plays a key role in the future adoption of PV along with the economics of both the manufacturer and the customer.

The reliability trend of a product can be depicted as a bathtub curve shown in Figure 1.1. The bath tub curve shows the product failure rates in three periods. The first one, infant mortality shows the failure rates when a product is launched. This can be reduced by qualification testing to identify the possible design flaws that might occur in the first few years in the field. The second period depicts the useful life, when defects are already identified and corrected. Failures occur randomly due to manufacturing quality control issues and the overall trend is at a constant rate. The failure rates are low in this period. The third period is the end-of-life period and the failure rate increases due to wear out failures.

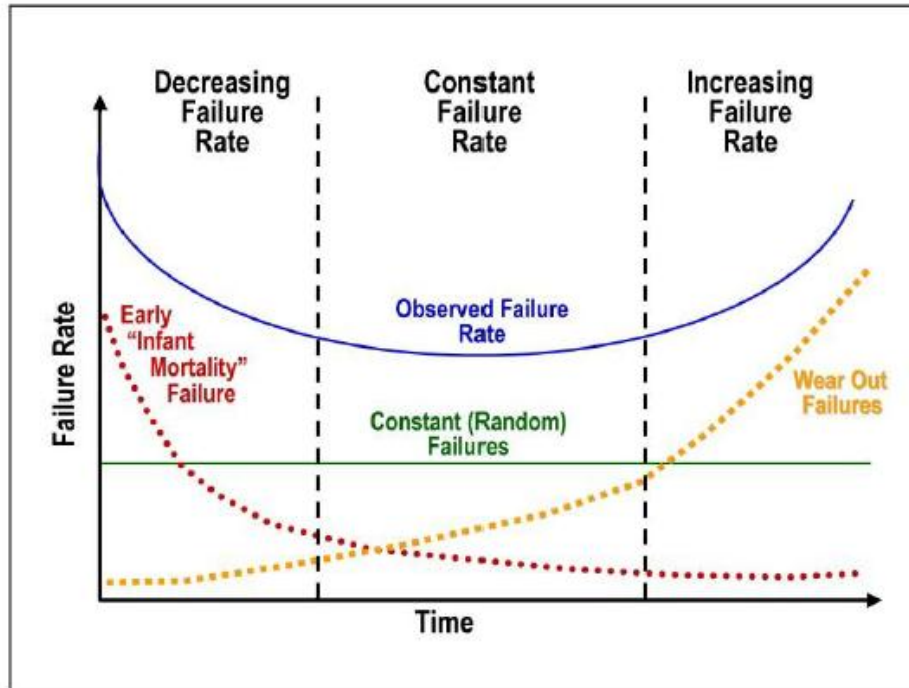


Figure 1.1: A Bath tub curve depicting failure rates at various periods in a products lifetime. [2]

The most fundamental element defining the degradation and reliability requirements is the level of applied stress. It has been reported that the following stresses play key roles in module degradation and reliability [1].

- Operating temperature
- Humidity
- UV exposure
- Operating voltage

The operating temperature has significant influence on hot-spots, encapsulant degradation, delamination, interconnect failure, etc. [1]. Most of the chemical reactions involved in degradations are a function of temperature [3].

The presence of humidity promotes corrosion, encapsulation degradation and delamination. It can also lead to large differential expansion of stresses that aggravate delamination and fatigue [1].

UV exposure could lead to encapsulant browning, depending upon the type of encapsulant used. System voltage has implications on the grounding requirements and electrochemical corrosions.

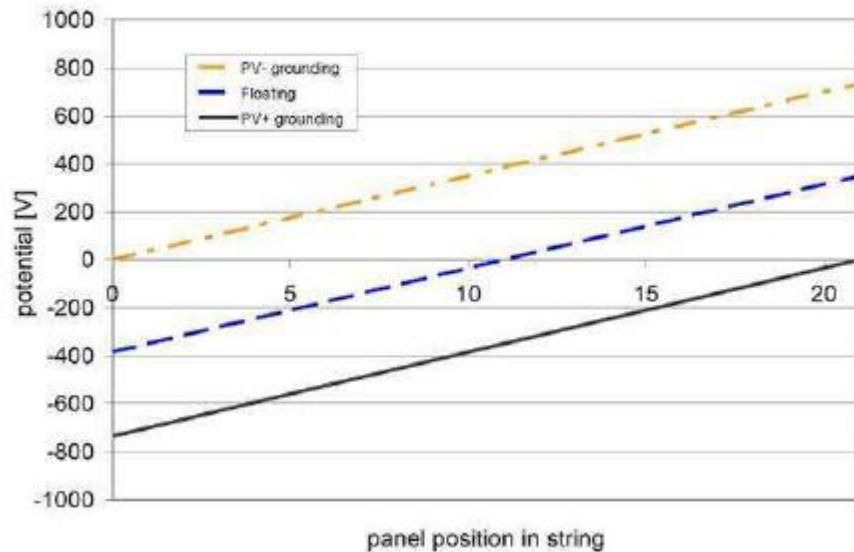


Figure 1.2: Voltage & polarity depending upon its position and grounding [4].

Figure 1.2 shows the voltage and polarity of a module depending upon its position in an array. As an example, the negative side of an array is grounded, the modules farthest from the grounding point is under a stress of  $+V_{SYS}$ , while the module closest to the grounding point is at 0 V. When the positive side is grounded, the farthest module is under a stress of  $-V_{SYS}$ , while the closest module is under 0 V. When the array is ungrounded (floating), the middle module is under 0 V stress, while each of the modules at the either end of the array is under  $+V_{SYS}$  and the other is at  $-V_{SYS}$  stress.



In typical crystalline silicon modules, potential induced degradation (PID) occurs in the modules closest to the negative voltage side of an array. The high potential difference between the cells and frame causes a polarization effect leading to leakage current discharged to the ground. Over a period of time and under the influence of high voltage, temperature and humidity, the leakage current causes potential induced degradation (PID) and reduces the module performance.

## 1.2 Statement of purpose

The basic difference between the PID evaluations carried out by ASU-PRL and other research laboratories is the history of the test modules. The other research groups have been using fresh modules for their PID evaluations whereas the research group at ASU-PRL has been using the accelerated stress tested modules to better simulate the behavior of actual field stressed modules which might be more susceptible to the PID losses. The accelerated stress tests are: damp heat test (1000 hours at 85°C/85%RH) and thermal cycling test (200 cycles) both per IEC 61215.

The previous studies carried out at ASU-PRL indicated that:

- The conventional crystalline silicon PV modules are not susceptible to PID losses due to positive voltage bias
- The conventional crystalline silicon PV modules are susceptible to PID losses due to negative bias. The PID losses are significantly greater when a carbon layer was used for the surface conductivity of the glass superstrates and are

lower when water layer from high humidity was used for the surface conductivity of the glass superstrates.

In the previous PID evaluations at ASU-PRL, the glass surface conductivity was extended to the frame by using either a carbon layer or water layer. In this study, the glass surface conductivity is disrupted near the frame edges to investigate if the PID can be interrupted just by interrupting the conductivity circuit close to the frame.

The objective of this thesis is to understand the performance degradation of two damp heat (DH 1000) and two thermal cycling 200 (TC 200) stressed modules under three different voltages, two different temperatures, and two different conditions of glass surface conductivity. The primary objective of this thesis is to investigate the effect of surface conductivity disruption on PID of PV modules.

### 1.3 Scope

PID effect on crystalline silicon (c-Si) modules can be reduced or eliminated by:

- By modifying anti-reflective (AR) coating of the cells
- By increasing the bulk conductivity of encapsulant
- By disrupting the glass surface conductivity

This work addresses the effect of surface conductivity disruption on PID.

Sandhya Goranti, worked on PID under high surface conductivity. This was achieved by applying a layer of conductive carbon paste on the front glass of a PV

module, with the paste touching the module frame. The results showed that modules degrade significantly under negative bias and a high surface conductivity [5]. Figure 1.3A shows an illustration of a module under high surface conductivity. Faraz Ebneali, worked on PID under low conductivity conditions. This was achieved by stressing the samples under a relative humidity of 85%. This work found that fresh samples compared to samples that were pre-stressed under damp heat (DH) for 1000 hours would degrade significantly greater than samples that were subjected to a thermal cycling (TC) pre-stress [6]. This research also concluded, that “degradation in negative bias depends on history (fresh, TC or DH) and surface conductivity [6].” Figure 1.3B shows a pictorial representation of a module under low conductivity condition.

The work of this thesis will disrupt the surface conductivity of PV modules and study its effect on PID. The surface conductivity is simulated by applying a layer carbon paste. The surface conductivity is disrupted by maintaining a 2 cm gap from the edges. Figure 1.3C shows a pictorial representation of a module, when its surface conductivity is disrupted.



Figure 1.3A: High Surface Conductivity (full surface carbon) [5]

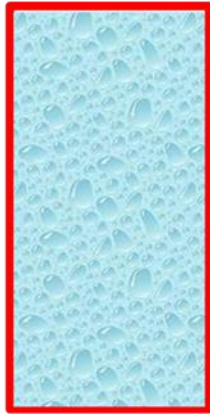


Figure 1.3B: Low Surface Conductivity (humidity) [6]



Figure 1.3C: Disrupted Surface Conductivity (simulated with partial carbon).

The scope of the current work includes the following:

1. Obtaining light current-voltage (I-V) curves of pre-stressed modules (damp heat [DH]– 1000 hours; Thermal cycling [TC] – 200 cycles).
2. Collecting dark I-V curves, electroluminescence (EL) and infrared (IR) images before the initiation of PID tests.
3. Performing PID on 3 projects each consisting of two DH 1000 modules and two TC 200 modules under varying:
  - a. Voltages (-300V, -400V and -600V)
  - b. Temperatures (60°C and 85°C)
  - c. Conductivity (full and partial surface conductivity of glass superstrate using conductive carbon paste)
4. Repeating steps 1 and 2 as the final measurements to determine the PID test induced defects and performance losses.

## CHAPTER 2

### LITERATURE REVIEW

Photovoltaics is the method of converting electromagnetic (EM) energy into electrical energy utilizing the photovoltaic effect. A solar cell is a semiconductor device, which contains an electron rich (N-type) layer(s) and a hole rich (P-type) layer(s) separated by a junction. The incoming photons energize the electrons, which move away from the junction and are collected by an external circuit [7]. According to Stephen Fonash [8], the basic four steps needed for photovoltaic energy conversion are:

- a) A light absorption process which causes a transition in a material (the absorber) from a ground state to an excited state,
- b) Conversion of the excited state into (at least) a free negative and a free positive-charge carrier pair, and
- c) A discriminating transport mechanism, which causes the resulting free negative-charge carriers to move in one direction (cathode) and the resulting free positive charge carriers to move in another direction (anode).
- d) Combining with an arriving positive-charge carrier, thereby returning the absorber to the ground state.

Figure 2.1 depicts an equivalent circuit for a PV cell with the load ( $I_L$ ), diode ( $I_D$ ) currents and the series ( $R_S$ ) & parallel ( $R_P$ ) resistances.

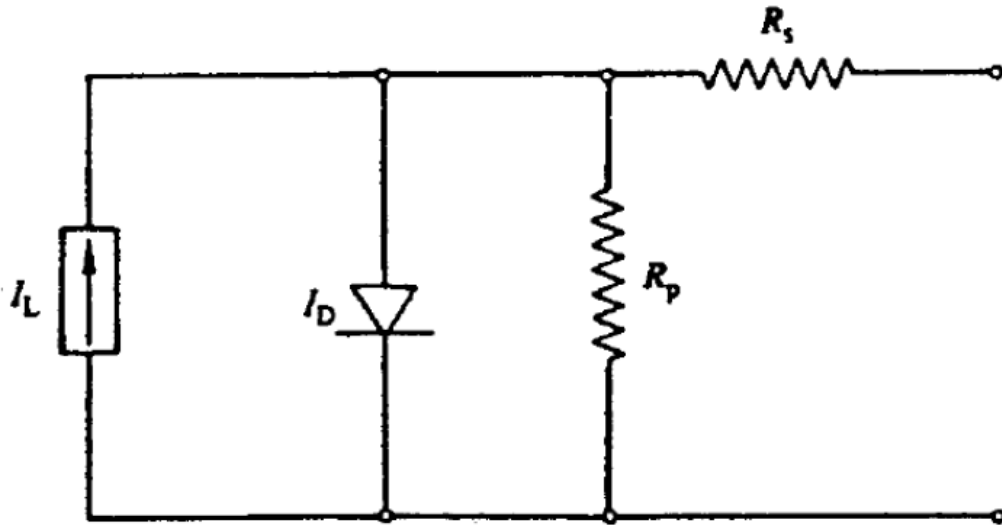


Figure 2.1: Equivalent circuit of a PV cell [7].

## 2.1 Reliability and acceleration testing

Reliability of an item is defined as the ability to operate under certain conditions for a certain period of time.

Reliability can be mathematically expressed as

$$R(t) = \int_t^{\infty} f(x) dx$$

Where R (t)-Reliability

t- Time period,

f(x)- Failure probability density function

Reliability studies help to understand failure rates, causes of failure, and the anticipated lifetime of a product, so that the manufacturer has a basic understanding of their product. Lifetime prediction and causes of failure through field tests require long periods of testing which is considered a luxury in today's

competitive market. To overcome this, increasing stress levels beyond the design limits or accelerated testing may be employed. This results in the acceleration of failures with the single purpose of quantifying of the life characteristics of the product at normal use [9]. Accelerated life testing can consist of two types, qualitative accelerated life testing and quantitative accelerated life testing [10].

#### 2.1.1 Qualitative Accelerated Life Testing

Also known as High Accelerated Life Testing (HALT), qualitative accelerated life testing reveals probable failure modes. A good qualitative test is one that quickly reveals those failure modes that will occur during the life of the product under normal use conditions [10]. HALT uses a "test-to-failure" approach employing temperature, vibration, and electrical stress exposure to rapidly precipitate and detect failures during the product development stage. Those test failures deemed relevant, or likely to cause field failures, are eliminated from the product [11].

#### 2.1.2 Quantitative Accelerated Life Testing

These tests are designed to quantify the life characteristics of the product. Reliability information can include the determination of the probability of failure of the product under use conditions, mean life under use conditions and projected returns and warranty costs. They can also be used to assist in the performance of risk assessments, design comparisons, etc. [10].

The following table shows the required acceleration test to simulate the field failure mechanisms.



Table 2.1: Relation between failure mechanism, field failure symptom and acceleration test [12].

<b>Failure Mechanism</b>	<b>Field Failure</b>	<b>Acceleration Test</b>
<b>Moisture Penetration</b>	Delamination	Damp heat Humidity freeze
<b>Moisture induced electro-chemical reaction</b>	Corrosion of cell metallization	Damp heat
<b>Thermal expansion and contraction</b>	Inter-connect breakage	Thermal cycling

## 2.2 Types of Acceleration Tests

The International Electro-Technical Commission (IEC) standard (IEC 61215 second edition), identifies several environmental stress tests [13], [12].

Two of the stresses used in this study are presented below:

### 2.2.1 Thermal Cycling (TC)

To determine the ability of the module to withstand thermal mismatch, fatigue and other stresses caused by repeated changes of temperature. Modules are connected to a power supply (positive to positive and negative to negative) and are thermally stressed for 200 cycles. The rate of change of temperature between the low and high

extremes shall not exceed 100 °C/h and the module temperature shall remain stable at each extreme for a period of at least 10 min. The cycle time shall not exceed 6 h unless the module has such a high heat capacity that a longer cycle is required [13] [12]. The number of cycles shall be as shown in the relevant blocks in the figure 2.2.

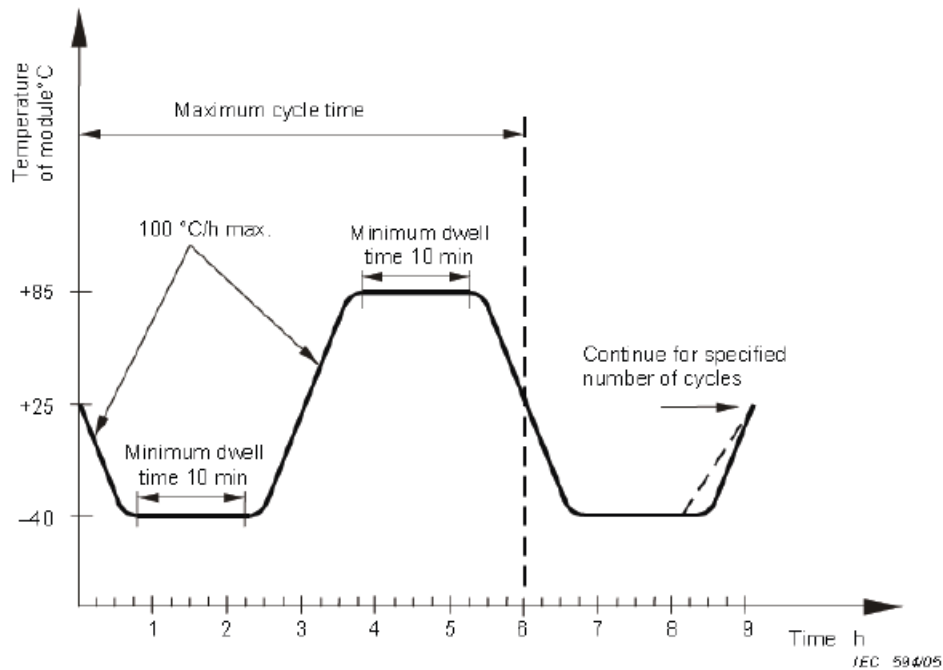


Figure 2.2: Temperature (°C) Vs. Time (h) for a thermal cycling stress test [13].

### 2.2.2 Damp Heat (DH)

To determine the ability of the module to withstand corrosion, delamination caused by moisture penetration in high temperature-high humidity environments. The modules are introduced into a chamber at room temperature and the temperature and humidity are slowly ramped up to 85 °C  $\pm$ 2 °C and 85 %  $\pm$ 5 %, and are maintained under these conditions for duration of 1000 hours [13] [12].

## 2.3 Types of Conductivity

As shown in Figure 2.4, the following three types of leakage paths could be observed in a module:

### 2.3.1 Surface Conductivity

Here, the leakage current travels across a conductive path established by the presence of moisture on the surface of the module.

### 2.3.1 Bulk Conductivity

It is conductance through the bulk of the material(s) that compose the module, e.g. Encapsulant.

### 2.3.2 Interface Conductivity

It is the conductance through the interface between two components, e.g. encapsulant/glass interface, encapsulant/cell interface and/or encapsulant/back sheet interface

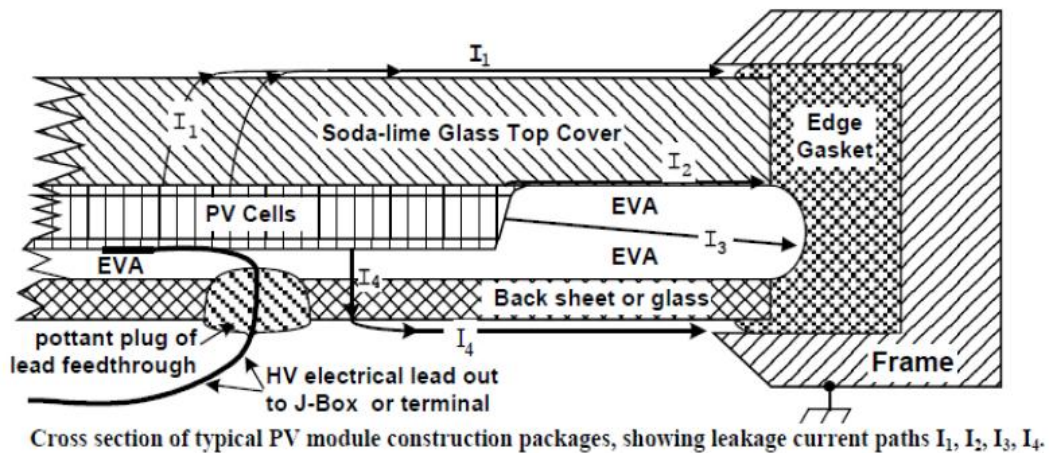


Figure 2.3: Leakage current pathways in a PV module [14].

The important leakage current (LC) pathways are depicted in the Figure 2.3, which shows conductance through the glass ( $I_1$ ) and along the interfaces or

EVA contained within the module package ( $I_2$ ,  $I_3$ ) and out to the frames  $I_4$ , which shows conductance through back sheet and which was recently identified as a possible path [14].

Under a high voltage bias, one of the leakage current paths becomes predominant due to the influence of environmental factors like humidity or temperature. Under very high relative humidity, leakage currents are dominated by path  $I_1$ , i.e. conductance through the front glass, along the outer surface of glass and then to the frame. This is due to a conductance by a layer of adsorbed water on the top surface [14]. Similarly due to high relative humidity (RH), the back sheet also gets coated with water and could become conductive ( $I_4$ ) [14].

Under a low humidity atmosphere and with a thin layer of carbon paste applied on the front surface,  $I_1$  will be the most prominent path, while the other three paths will have negligible/ zero conductance.

#### 2.4 Potential Induced Degradation (PID)

Potential induced degradation occurs in p-type wafer based crystalline silicon modules under a negative bias [15]. This may be due to a positive charge moving towards the active area from the grounding point [16]. Positive sodium ions ( $\text{Na}^+$ ) are deposited onto the active area, thus reducing the fill factor.

Investigations of cell fragments on microstructural level show an accumulation of alkali metals within the  $\text{SiN}_x$  anti-reflective layer, as well as at the interface to the Si. At the same location, changes of the p-n junction properties are observed [17].

This is believed to be associated with the decomposition of silicon nitride to hydrous silica and ammonia in the presence of high chemical activity of water

[18]. This can be reduced by increasing the resistivity of glass and encapsulant [16]. Also, by increasing the refractive index of the anti-reflective coating, PID could be mitigated [4].

Photovoltaic modules in the field maybe connected in series to reach the required high voltages. The typical maximum system voltage ( $V_{sys}$ ) for series connection is 600V (United States) and 1000V (Europe). These high voltages may allow leakage currents between cell and frame/metallic mountings. High leakage current leads to electrochemical degradation. Environmental factors like temperature and humidity can have significant impact on leakage currents.

Leakage currents may be potentially dangerous to workers and are also responsible for degradation due to electrochemical corrosion. Electrochemical reaction rate is proportional to the rate of inter electrode ionic charge transfer. Moisture present in the atmosphere plays an important role in PID.

Research work [5], [6] at Arizona State University's Photovoltaic Reliability Laboratory (ASU-PRL) indicate that pre-stressed modules (DH1000 and TC200) experience practically no degradation at +600 V when the surface conductivity of glass is extended to the frame using a conductive carbon paste or ambient humidity (Figure 2.4). However, they degrade at -600 V when the surface conductivity of the glass is extended to the frame using the conductive carbon paste or ambient humidity (Figure 2.5).

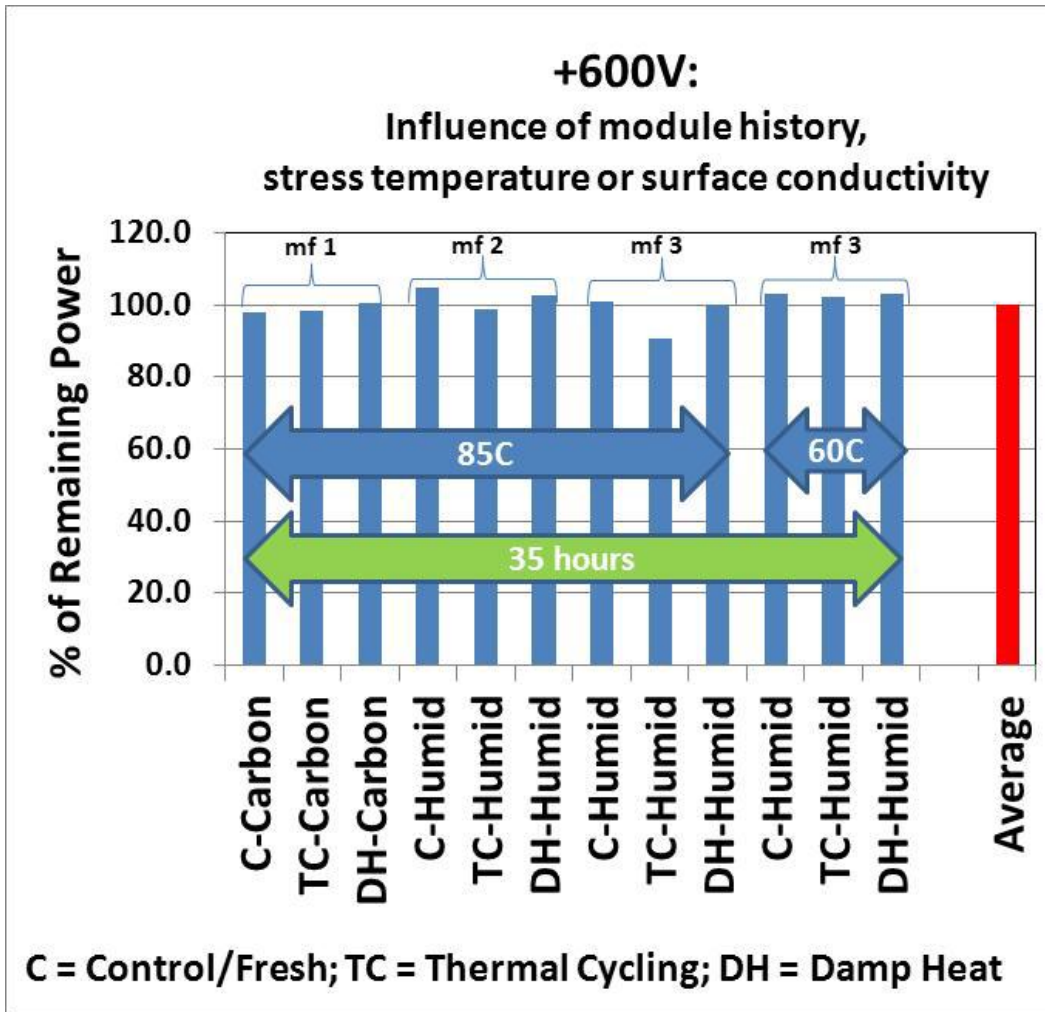


Figure 2.4: Influence of full surface conductivity (carbon or humidity) of glass on PID at +600 V

[6].

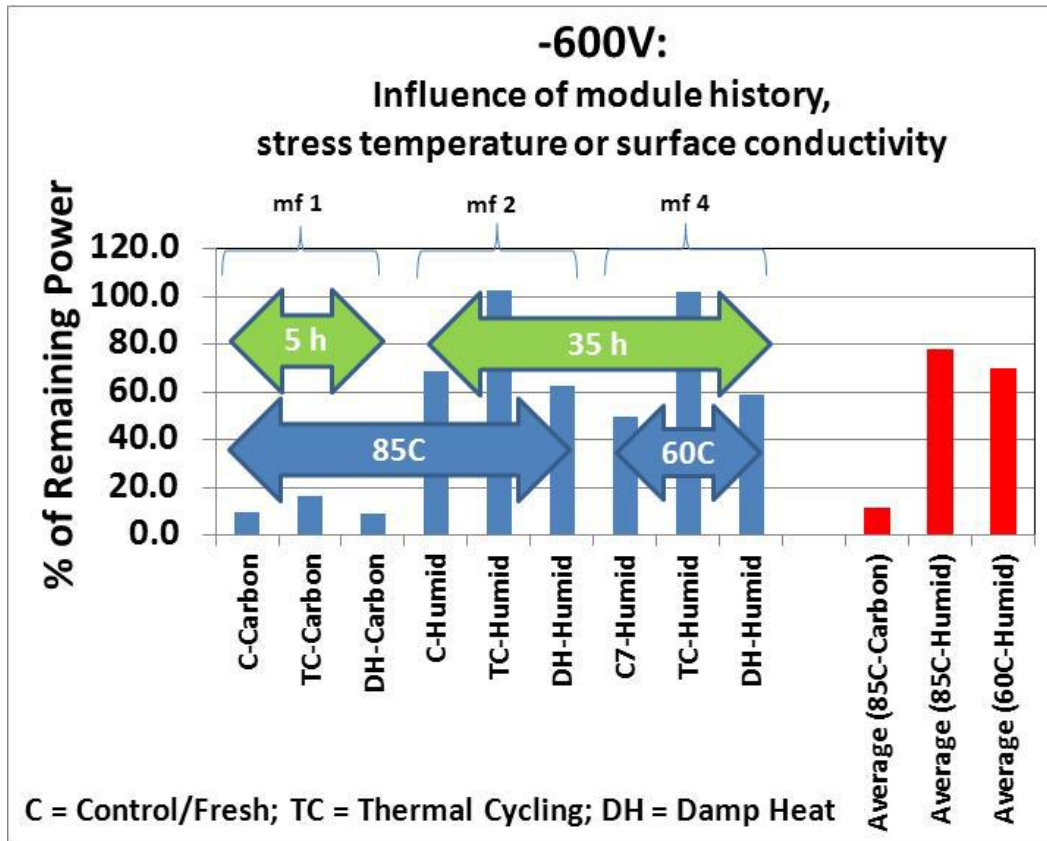


Figure 2.5: Influence of full surface conductivity (carbon or humidity) of glass on PID at -600 V (since the surface conductivity of carbon is higher than water layer (due to humidity), carbon coated modules degrade at higher rate) [6].

Concurrently, according to other research work performed by ASU-PRL for hot-dry climatic conditions of Tempe/Arizona, the actual power plant modules under positive system voltage (negative grounded) did not exhibit PID as explained below [19]. A total of 1155 modules were connected in 55 strings of 21 modules each. Figure 2.6 shows a string circuit diagram for a typical array at the aforementioned site. Considering, the negative end of each string was centrally grounded, making the string positively biased. Module 1 is under lowest level of potential, while module 21 has the highest level of potential impressed across it

[19].

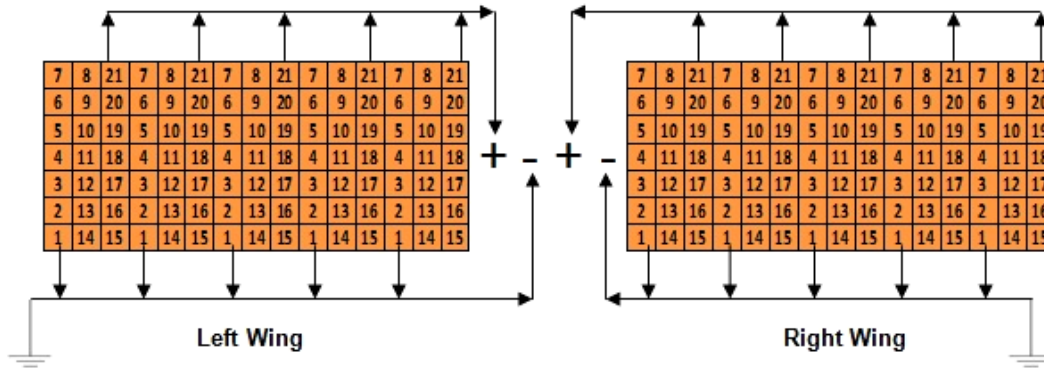


Figure 2.6: String circuit diagram for an array at APS-STAR facility [19].

Figure 2.7 plots degradation percentage of all 1155 modules with respect to their position in the string, with each data point corresponding to 55 modules. The total number of strings exhibiting an increasing slope, decreasing slope and constant slope of power degradation with respect to position in a string were 18, 24 and 13 respectively. Thus, no real trend on an average was observed [19]. PID mechanism does not seem to be responsible for degradation + bias: Modules degrade at 0.6-2.5% per year, but the PID does not seem to be responsible for the degradation of negative grounded systems in the hot-dry climatic condition of Phoenix, Arizona.



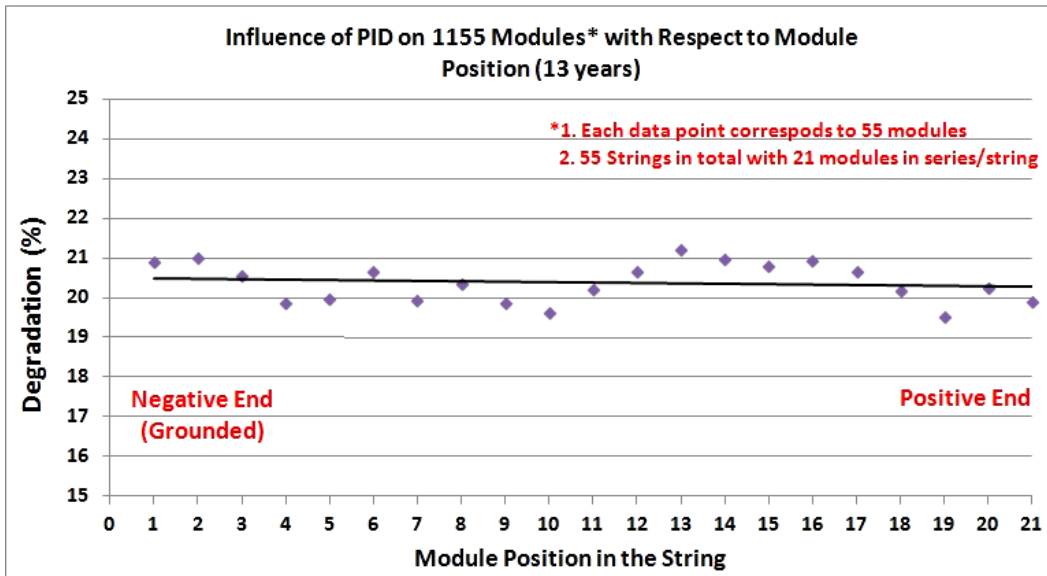


Figure 2.7: Influence of PID on 1,155 modules with respect to module position in the string.

Overall: No Specific Trend could be observed.

## CHAPTER 3

### METHODOLOGY

This chapter describes the methodology applied to evaluate PID effects on PV modules. As shown in Figure 3.1, the test modules were subjected to pre-characterization, PID stress and then post-characterization. Before the pre-characterization tests were carried out, the test modules were pre-stressed either for thermal cycling condition (200 thermal cycles) or damp heat condition (1000 hours) according to IEC standard 61215. The thermal cycling or damp heat pre-stressing was carried out to simulate the field aged modules.

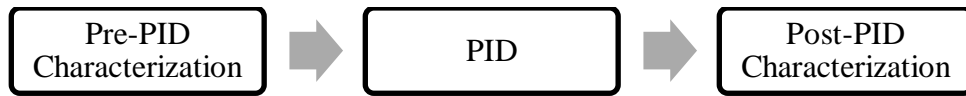


Figure 3.1: Overall methodology followed during PID stress testing.

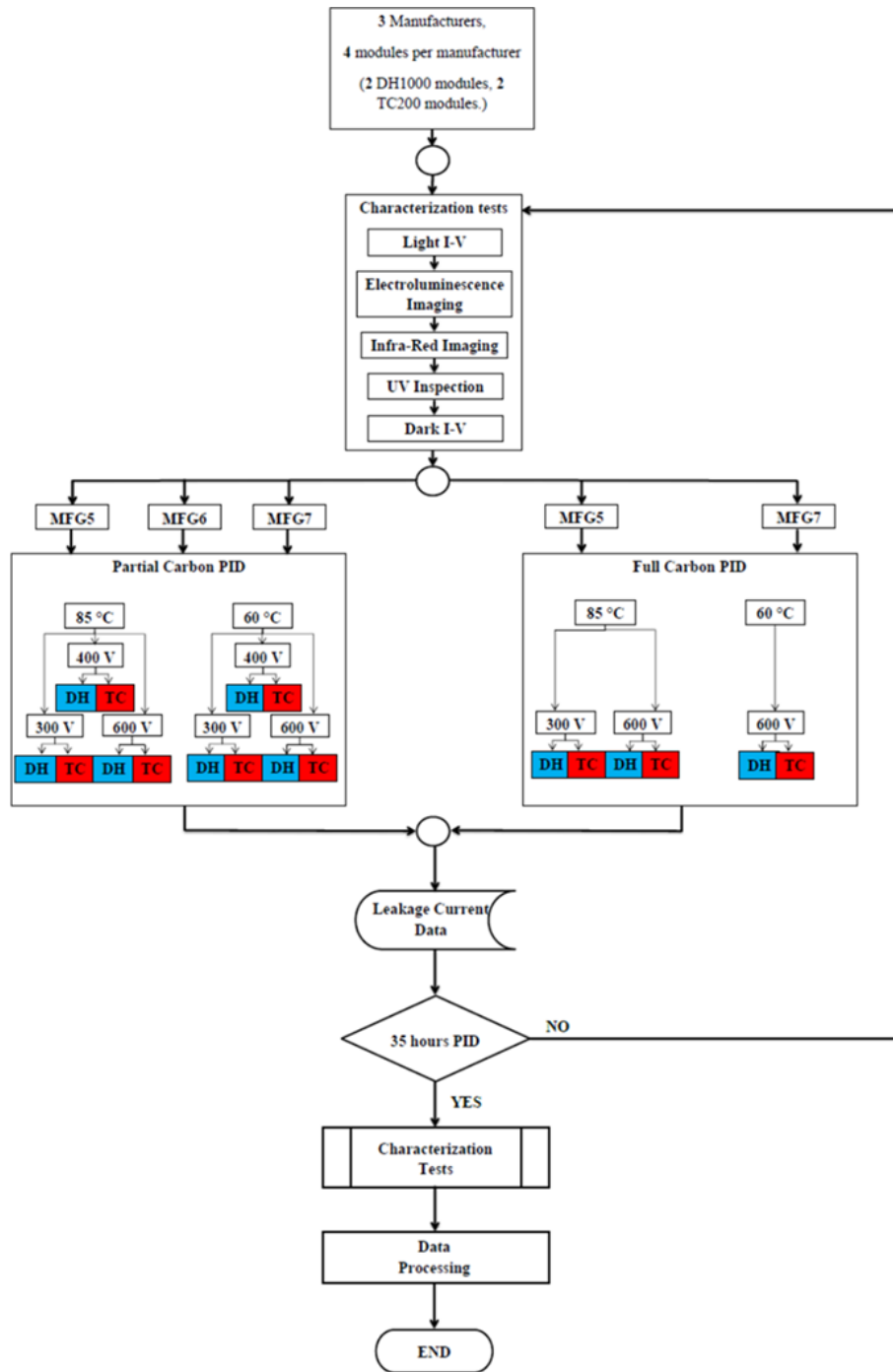


Figure 3.2: Flow chart.

### 3.1 Characterization

As shown in Figure 3.3, four characterizations were carried on every test modules before PID, during PID and after PID. Additionally, they were carried out after potential induced recovery (PIR).

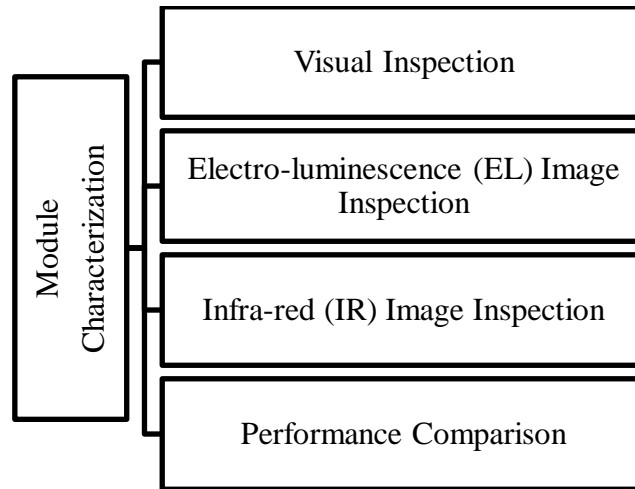


Figure 3.3: Characterization of modules.

#### 3.1.1 Visual Inspection

Modules were visually inspected for any physical defects according to *Crystalline silicon terrestrial photovoltaic modules- Design qualification and type approval*, IEC 61215-2: 2005 [13]. Modules are inspected under natural sunlight for the following major defects.

- Broken/ cracked cells
- Broken superstrate or substrate
- Bubbles or delamination



Figure 3.4: Visual inspection was performed under natural sunlight

The above figure 3.3 shows a module undergoing visual inspection under natural sunlight to identify any visual defects mentioned earlier.

### 3.1.2 Electro-luminescence (EL) Image Inspection

Electro-luminescence (EL) relies on the same principle as a light emitting diode (LED). Current is fed into the module and radiative recombination of carriers causes light emission. As an indirect semiconductor, most of the recombination in silicon occurs via defects [20]. The emission is relatively low, but can be captured using a camera, which is sensitive to near IR radiation. The following procedure was used to take EL images at ASU-PRL.

1. Module is placed in a dark room with its superstrate facing the camera.
2. The module is connected to a power supply in a forward biased condition.

3. A constant current equaling to 1.3X the module  $I_{SC}$  is injected into the module for a few minutes.
4. Using a coolSamba HR-830 camera manufactured by Sensovation AG, EL images are captured.
5. The image is studied in detail to identify any defects.

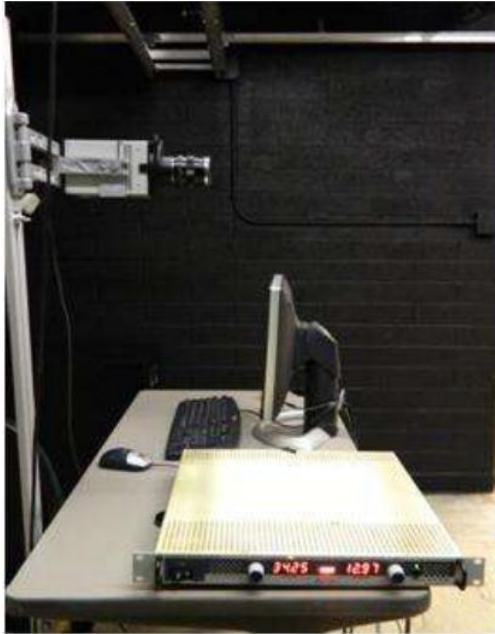


Figure 3.5: An EL camera, a power supply and a computer are used to capture EL images.



Figure 3.6: A module is shown on an adjustable rack in front of the EL camera.

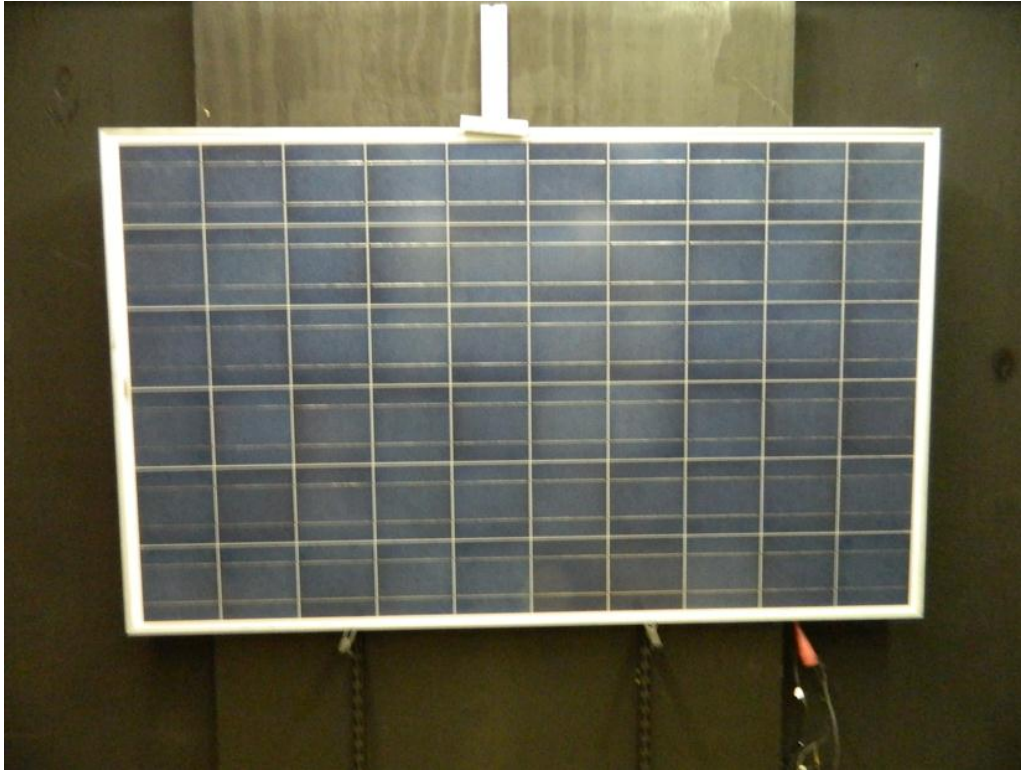


Figure 3.7: A module is shown to be placed securely on the rack.

Figures 3.4 and 3.5 show the EL imaging studio at ASU-PRL. It comprises of aforementioned equipment like an EL camera, a power supply and a computer along with an adjustable rack for mounting the test sample. Figure 3.6 shows a close-up of the module on its rack. Figure 3.7 shows a sample EL image, it is clearly seen that some cells in the module have turned darker or even stopped emitting. These are the problem areas, where the cells are dead. Modules are also thoroughly studied using IR and UV images to corroborate these findings.

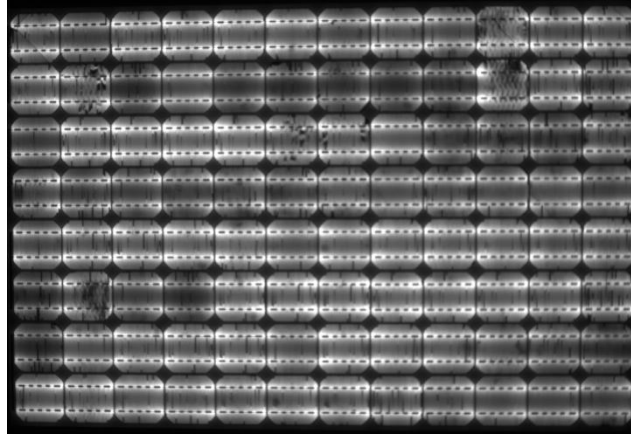


Figure 3.8: EL images are taken before, during and after PID and recovery.

### 3.1.3 Infra-red (IR) Image Inspection

A typical solar module converts only 10-20 % of the incident irradiance, while the rest is either reflected, or dissipated as heat, and electromagnetic radiation. Defects like hot-spots could be easily detected using an IR camera. The following procedure has been followed to capture IR images of the modules.

1. Module is placed on tracker/ roof-top under a natural irradiance of not less than  $1000 \text{ W/m}^2$  [13].
2. Leads of the module are shorted and the module is exposed to irradiance for about 5-10 minutes.
3. Using a Ti55FT IR camera, manufactured by Fluke Corporation, images are captured.

Capturing the images during 11AM-2PM on a clear sunny day with a wind speed of 1m/s, would see that the images free from errors caused by environmental factors. Figure 3.8 shows an IR image for a test sample.



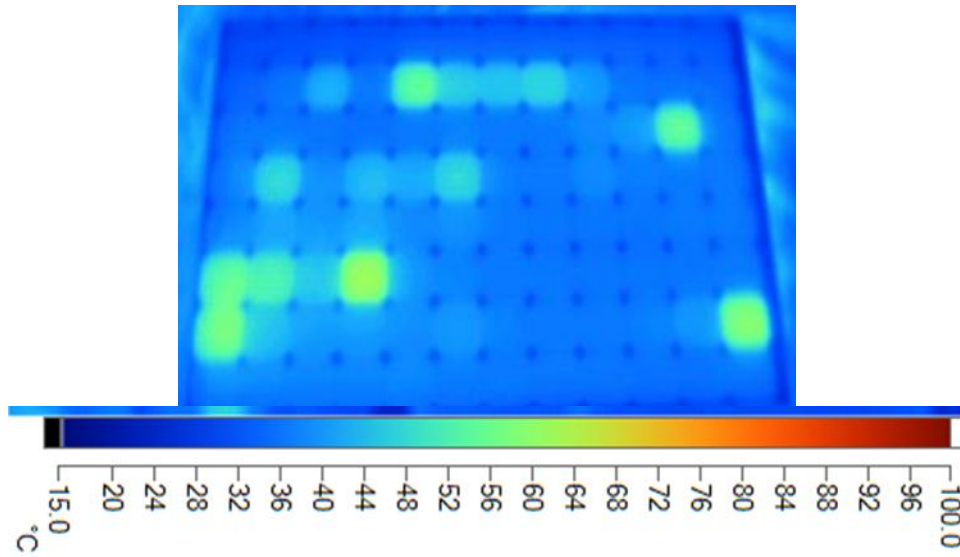


Figure 3.9: An example of an IR image of a module along with temperature scale.

### 3.1.4 Performance Comparison

The IV curve of a solar module is the superposition of the IV curve in the dark with the light-generated current. Figure 3.6 shows the effect of light on the current-voltage characteristic on a p-n junction diode. The IV curve of a solar cell is the superposition of the IV curve of the solar cell diode in the dark with the light-generated current. The light has the effect of shifting the IV curve down into the fourth quadrant where power can be extracted from the diode. Illuminating a cell adds to the normal "dark" currents in the diode so that the diode law becomes

$$I = I_0 \left[ \exp\left(\frac{qV}{nkT}\right) - 1 \right] - I_L$$

I- Total current (A)

$I_0$ - Saturation current of the diode (A)

$I_L$ - Light generated current (A)

V- Cell voltage (V)

q- Elementary charge ( $1.6 \times 10^{-19} \text{ C}$ )

n- Ideality factor (usually 1 or 2)

k-  $1.38 \times 10^{-23} \text{ J/K}$

T- Cell temperature (K)

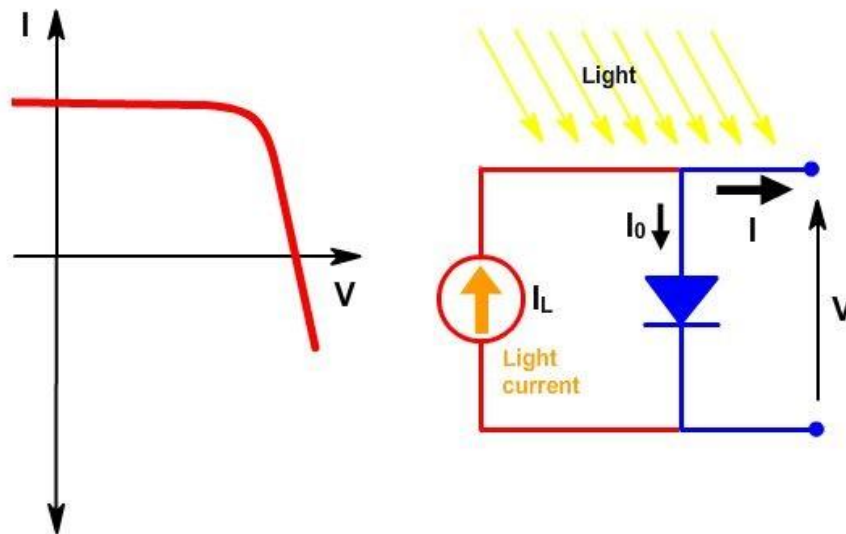


Figure 3.10: The effect of light on the current-voltage characteristics of a p-n junction [21].



Figure 3.11: Daystar DS 100 IV curve tracer (top-left), Reference cells (top-right), Sundial (bottom).

An IV curve tracer is able to provide both a qualitative visual representation and a quantitative measure of PV performance. In brief, a curve tracer uses a capacitive load to vary the impedance connected to the output terminals of the PV module [22]. Figure 3.7 shows the curve tracer used, along with reference cells to measure the irradiance, and a sun dial (in-plane with the module) used to keep the modules normal to the radiant beam.

The current-voltage characteristic of the module was measured using a DS100 IV curve tracer, manufactured by Daystar, Inc. The performance was measured under natural sunlight when the irradiance was above  $900 \text{ W/m}^2$  and module temperature varying between  $20 \text{ }^\circ\text{C}$  and  $50 \text{ }^\circ\text{C}$ . The following procedure is followed for performance measurements.

1. Module was initially placed in an environmental chamber and cooled down to about  $15 \text{ }^\circ\text{C}$ .
2. Module was then placed on a tracker under natural sunlight, with the tracker facing normal to the radiant beam. This can be achieved with the help of a sundial.
3. The module was connected to the curve tracer and at least 10 curves are taken between  $20 \text{ }^\circ\text{C}$  and  $50 \text{ }^\circ\text{C}$ .
4. A reference cell was used to measure the irradiance.
5. Ambient air and reference cell temperatures were also duly recorded.

Since photovoltaic system performance depends on irradiance and operating temperature, normalizing is used to translate IV curves taken at one set of irradiance and temperature conditions to a different set of irradiance and

temperature conditions. This is done so that IV curves taken under different conditions can be compared as if they were taken under identical conditions. Usually curves are normalized to standard conditions of irradiance at 1000 W/m<sup>2</sup> and temperature at 25 °C. ASTM E 1036 1996 method was used to normalize the IV curves using IVPC 3.0.5 software. The average powers after each test are then compared to determine the power loss of the module due to PID. Figure 3.8 shows a screen shot of the IVPC 3.0.5 software, which was used to collect IV curves and normalize them.

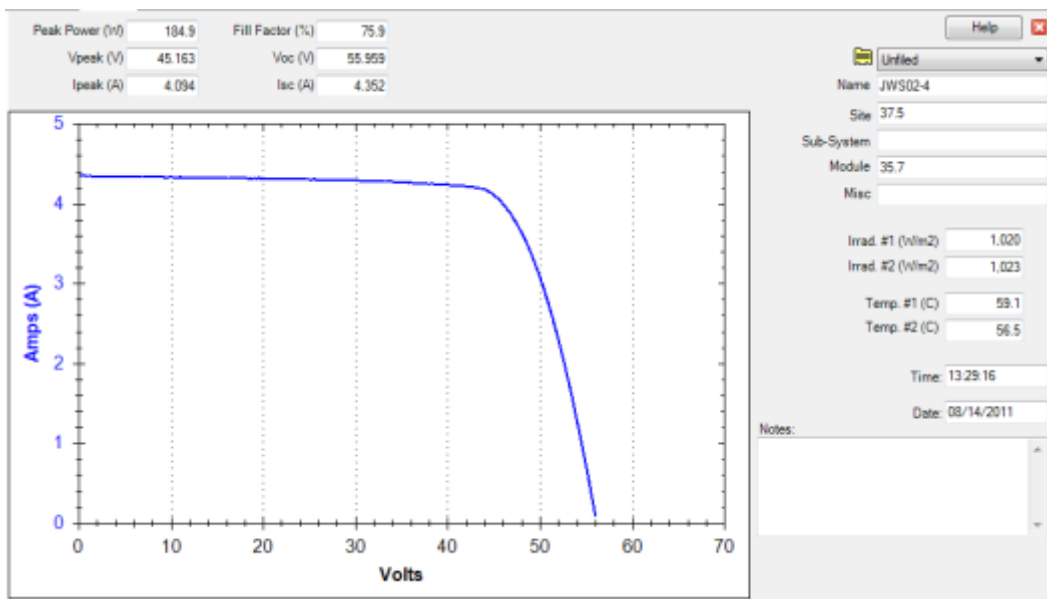


Figure 3.12: Performance measured using IVPC 3.05 software.

## 3.2 PID Stress

The following steps describe the equipment used, and the procedure followed to induce PID stress on modules.

### 3.2.1 Equipment/Material Used

#### a) Keithley 2700 data acquisition system

A Keithley 2700 data logger shown in Figure 3.9 having a resolution of 0.1  $\mu\text{V}$  is used to measure the leakage current in the circuit [23]. The voltage across a resistor in the PID box is measured and the leakage current is calculated using Ohm's law.

$$I = V/R$$

I-Leakage current (A)

V-Voltage across the resistor (V)

R-Resistance of the resistor ( $\Omega$ )



Figure 3.13: A keithley 2700 data logger used in the experiments. [24]

b) PS350 high voltage power supply

A power supply having a range of  $\pm 50$  V to  $\pm 5$  kV and a maximum current of 5 mA is used to induce high voltage on the samples. Figure 3.9 shows the front control panel of the Stanford Research Systems, PS350 power supply. It is capable of producing 25 Watts at a maximum voltage of 5000 V.



Figure 3.14: Front side control panel of the PS350 power supply.

c) PID Resistor Box

Since the leakage current in the circuit is beyond the sensitivity of the datalogger, voltage across a known resistance is measured instead and the leakage current is calculated using Ohm's law. It consists of a series of resistors in the circuit in between the module and the power supply. The 100 k $\Omega$  resistors act as a safety device to protect the power supply during fault situation, while voltage measured across the 5 k $\Omega$  resistor is used to calculate the leakage current. Figure 3.11 shows the circuit diagram of the PID resistor box.

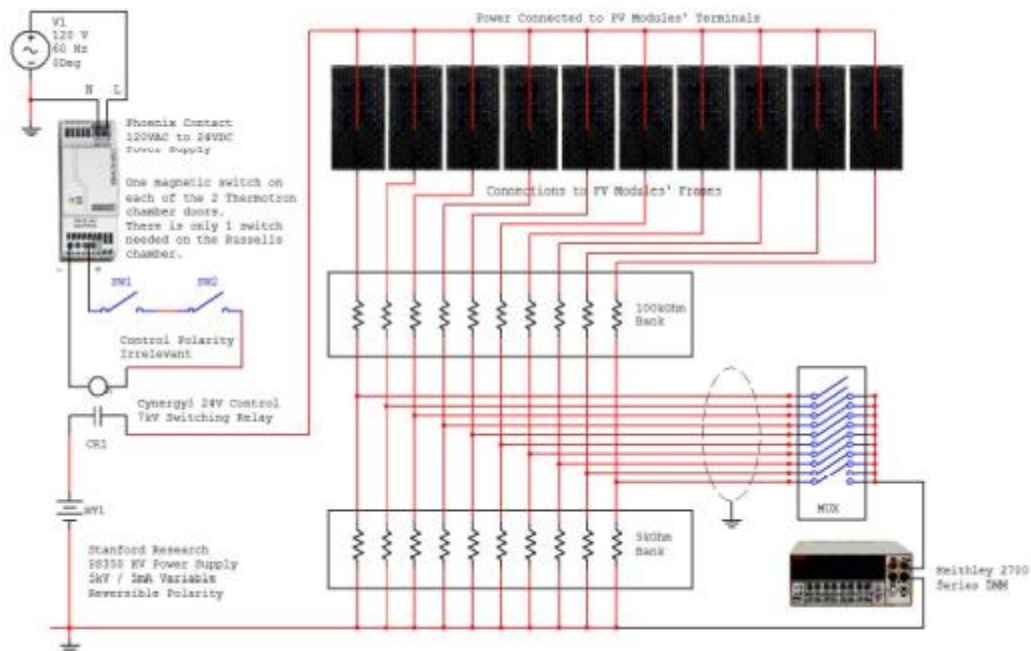


Figure 3.15: Circuit diagram of the PID box showing the modules, resistors, and the power supply [25].

#### d) Carbon paste

Under damp conditions, a thin but continuous layer of moisture is formed on the front glass of the module. As mentioned in the literature review, a leakage path could be established due to this layer. To simulate this, a thin layer of a conductive carbon paste is applied on the front glass of the module.

The carbon paste used in the experiments is MG Chemicals “846 carbon conductive paste,” having an electrical resistivity of  $117 \Omega \cdot \text{cm}$  and conductivity of  $8.57 \text{ mS} \cdot \text{cm}$ .



Figure 3.16: Modules hanging from ceramic insulators on a rack.

### 3.2.2 Procedure

- The superstrate of the module was covered with a thin layer of conductive carbon. . The carbon layer was extended from the glass surface to the frame for certain number of modules (referred as “full carbon”). For the other modules, in order to disrupt the conductivity/continuity, the carbon layer was not extended to the frame and the layer coverage was stopped 2 cm away from the edge of the frame (referred as “partial carbon”).
- The module was then placed in an environmental chamber on a rack as shown in figure 3.12. The modules are separated from the rack by ceramic insulators and teflon strips.
- Module leads was shorted and connected to the negative lead of the power supply, while the positive from the power supply is



connected to the grounding point on the module as shown in figure 3.13.



Figure 3.17: Positive from the power supply is connected to the grounding point.

- The power supply was turned ON and the required negative voltage (see Table 3.2) was applied.
- Temperature inside the chamber is increased at a rate of 1 °C/min
- The temperature and voltage were maintained for a total duration of 35 hours. In case of Mfg5 & 6, they are tested in two cycles of 5 hours, and one cycle of 25 hours.
- The temperature was decreased to ambient temperature at a rate of 1 °C/min.
- Voltage is turned OFF.
- Module performance was measured and compared with previous performance.

Table 3.1: Table describing the project parameters.

<b>Project</b>	<b>Group</b>	<b>Temperature (°C)</b>	<b>Voltage (V)</b>
<b>Mfg5</b>	1	85	-300 V
	2	60	-300 V
<b>Mfg6</b>	1	85	-400 V
	2	60	-400 V
<b>Mfg7</b>	1	85	-600 V
	2	60	-600 V

Table 3.1, provides, the stress parameters to be used for the test samples.

## CHAPTER 4

### RESULTS AND DISCUSSION

This chapter contains experimental results and data analysis. The catastrophic effects of carbon paste touching the frame was identified and the test procedure was modified to compare the test results obtained between the partial carbon coating condition and the full carbon coating condition.

#### 4.1 Partial Carbon

The modules were coated with a thin layer of carbon layer to increase their surface conductivity as shown in Figure 4.3. However, the paste was applied on the glass surface in such a fashion that it did not come into contact with the module frame. A space of 2 centimeters was maintained between the inner edge of the frame and the boundary of carbon coating. This coating method basically disrupted the continuity of the surface conductivity from the glass to the frame.

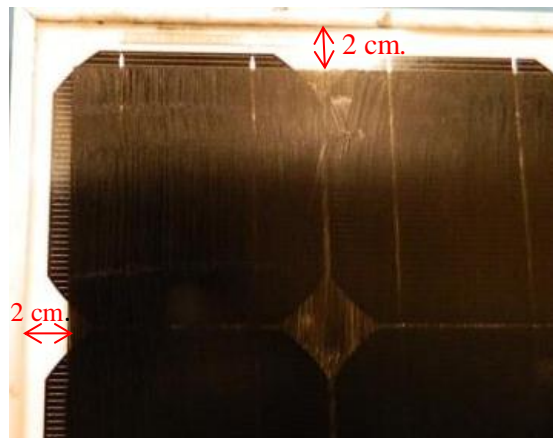


Figure 4.1: Frame without carbon coating; Glass with carbon coating;

The modules were stressed at various voltages and temperatures with this interrupted surface conductivity. Table 4.3 and Figure 4.4 show the performance results of modules before and after PID stress test at 60 °C.

Table 4.1: Performance comparison after PID under partial carbon condition at 60 °C.

	<b>Before partial carbon PID (W)</b>	<b>After partial carbon PID (W)</b>	<b>% of Power remaining</b>	<b>Applied Voltage (V)</b>	<b>PID Duration (hours)</b>
<b>Manufacturer 5</b>					
TC2	226.9	225.3	99.3	-300	35
DH2	192.5	182.7	94.9		
<b>Manufacturer 6</b>					
TC2	197.6	193.6	98.0	-400	35
DH2	180.0	180.2	100.1		
<b>Manufacturer 7</b>					
TC2	191.6	192.8	100.6	-600	70
DH2	168.7	165.8	98.3		
Average			98.53		

It can be seen that on average, the modules lost less than 1.5 % of their initial power due to PID stress at 60°C irrespective of manufacturer (Mfg 5, 6 or 7), stress voltage (-300, -400 or -600 V) or history of accelerated stressing (DH or TC). Two modules (a DH and a TC) have shown a slight increase in their output after 70 hours of PID. One module is a mono-silicon module stressed at -600 V, while other is a poly-silicon module stressed at -400 V. The power increase, although very small (less than 0.6%), might be due to measurement repeatability error and it is within the practicing industry standard limit of 1%.

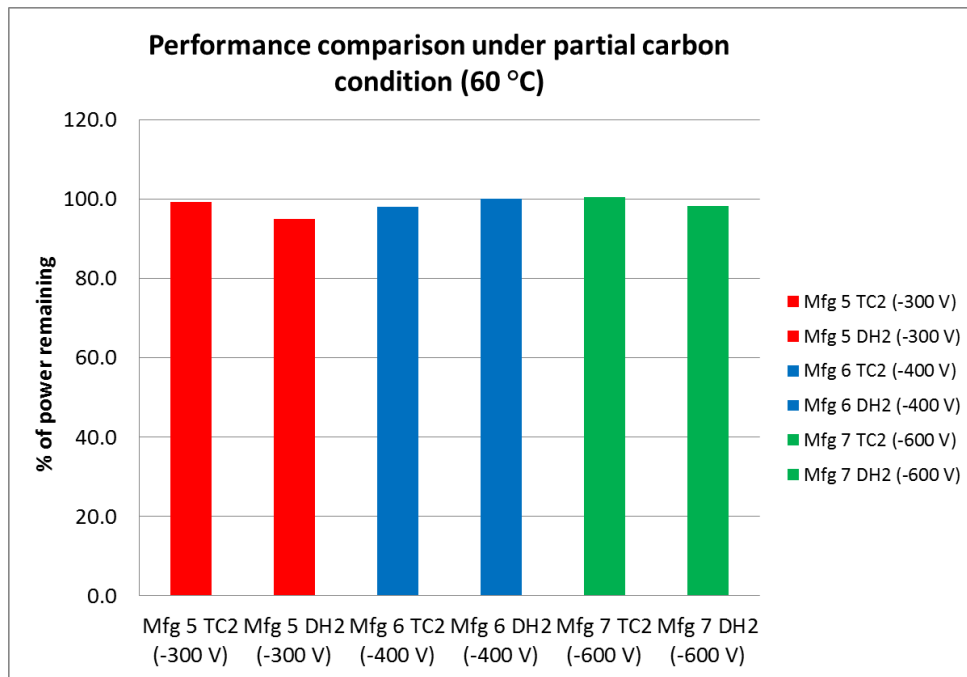


Figure 4.2: Performance comparison after PID under partial carbon condition at 60 °C for 70 hours.

Table 4.4 and Figure 4.5 show the performance results of the modules under partial carbon condition at 85 °C. It can be seen that on average, the modules lost less than 0.20 % of their initial power due to PID stress at 85°C irrespective of manufacturer (Mfg 6 or 7), stress voltage (-400 or -600 V) or - history of accelerated stressing (DH or TC).

Table 4.2: Performance comparison after PID under partial carbon condition at 85 °C.

	Before partial carbon PID (W)	After partial carbon PID (W)	% of Power remaining	Applied Voltage (V)	PID Duration (hours)
<b>Manufacturer 6</b>					
TC1	194.0	198.4	102.3	-400 V	35
DH1	205.8	199.5	96.9		
<b>Manufacturer 7</b>					
TC1	205.3	201.9	98.3	-600 V	70
DH1	176.4	179.4	101.7		
Average			99.8		

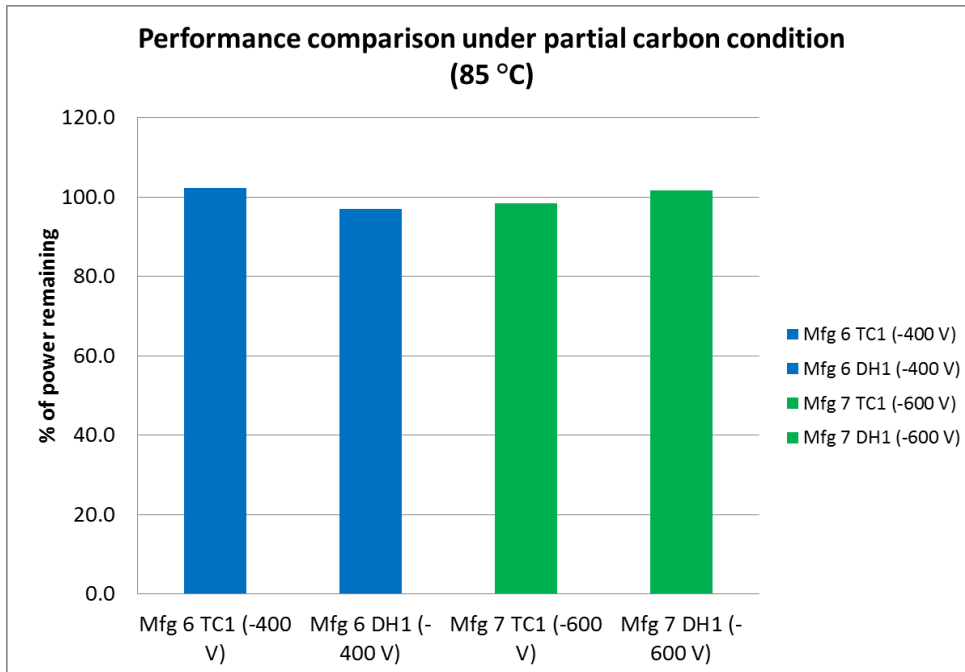


Figure 4.3: Performance comparison after PID under partial carbon condition at 85 °C.

## 4.2 Full Carbon

In the full carbon condition, the modules were completely coated with a thin layer of carbon paste to increase their surface conductivity, unlike the partial carbon condition, where the paste did not come into contact with the module frame. The photograph shown in Figure 4.4 provides a view of a module completely (both glass and frame) coated with carbon paste. It should be noted that these modules from manufacturer 7 (mfg 7) already underwent 70 hours of PID stress under partial carbon coating condition testing and they were reused to see the effect of full carbon coating on the glass and frame.



Figure 4.4: Frame with carbon coating; glass with carbon

Table 4.3 and Figure 4.5 show the performance results of modules before and after PID stressing at -600 V and 60 °C for 35 hours. It is seen that the TC and DH modules retain only about 67.0 % and 16.2 % of their pre-stress power. The average drop for two modules (MFG7: TC1, DH1) due to full surface conductivity at 60 °C is about 58.4%, whereas, it is only less than 0.6% average



power drop due to interrupted/partial surface conductivity. In comparison, the average power drop due humidity is about 30% [6].

Table 4.3: Performance comparison after PID under full carbon condition at 60 °C.

	Before full carbon PID (W)	After full carbon PID (W)	% of Power remaining	Applied Voltage (V)	PID Duration (hours)
<b>Manufacturer 7</b>					
TC	192.8	129.2	67.0	-600	70 hours (partial carbon coating) + 35 hours (full carbon coating)
DH	165.8	26.8	16.2		

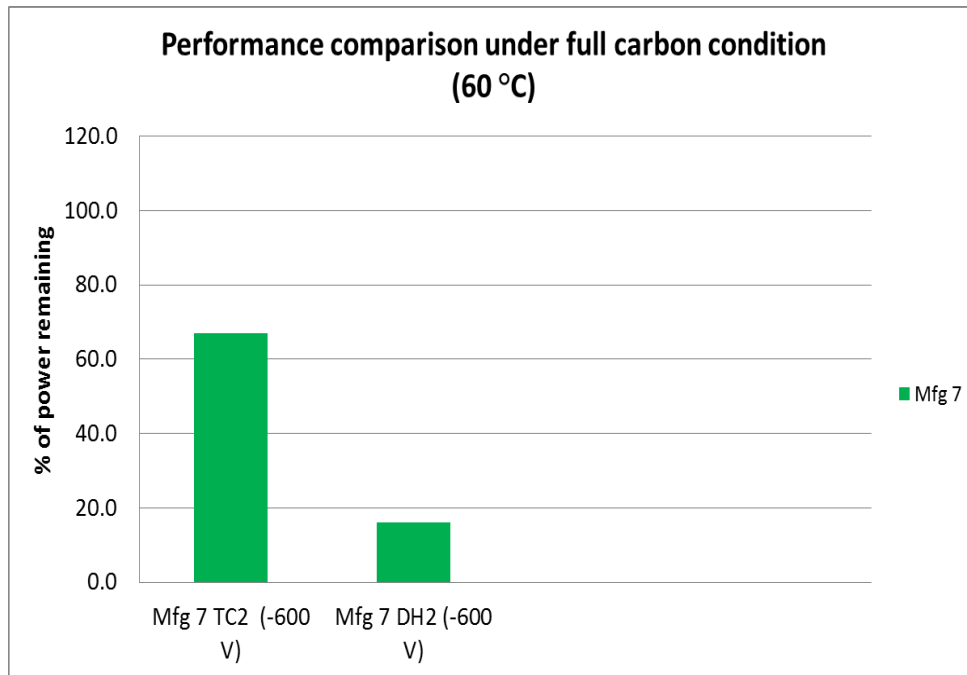


Figure 4.5: Performance comparison after PID under full carbon condition at 60 °C.

Table 4.4 and Figure 4.6 show the performance results of the modules stressed at 85 °C under full carbon condition. All the modules are mono-silicon

modules with two from Mfg 5 stressed under -300 V and two from Mfg 7 stressed under -600 V.

Table 4.4: Performance comparison after PID under full carbon condition at 85 °C.

	Before full carbon PID (W)	After full carbon PID (W)	% of Power remaining	Applied Voltage (V)	PID Duration (hours)
<b>Manufacturer 5</b>					
TC	201.6	80.4	39.9	-300	35
DH	186.1	8.8	4.7		
<b>Manufacturer 7</b>					
TC	201.9	60.5	30.0	-600	70 hours (partial carbon) + 35 hours (full carbon)
DH	179.4	14.2	7.9		

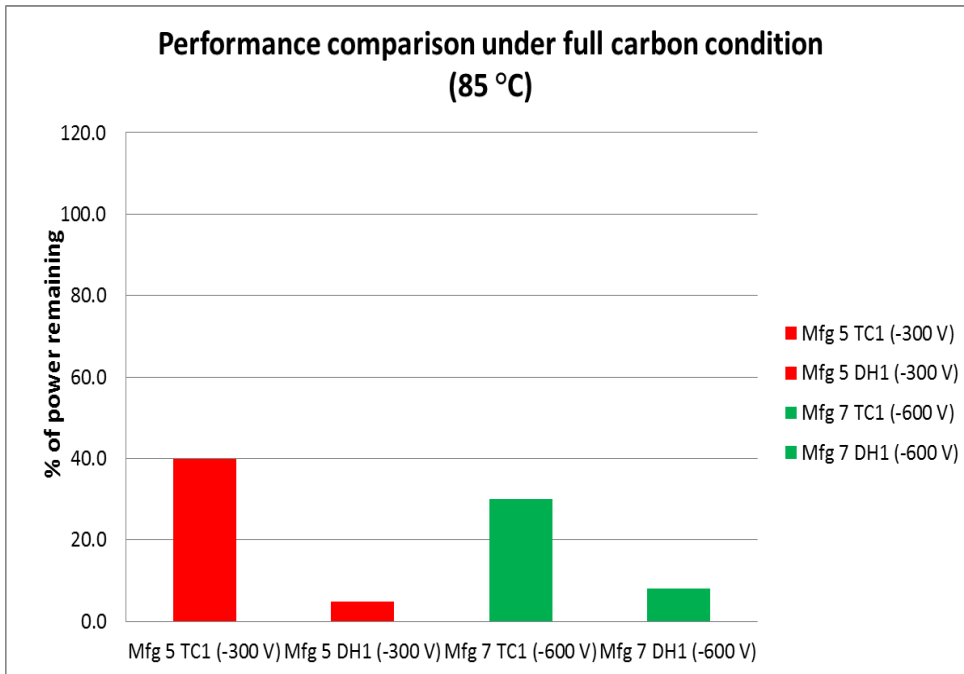


Figure 4.6: Performance comparison after PID under full carbon condition at 85 °C.

From Table 4.4 and Figure 4.8, it is shown that the modules have lost significant amount of power, with the DH modules losing more than the TC modules. This was expected and was also reported by Sandhya Goranti [5] and Faraz Ebneali [6].

The average power drop for four modules (MFG5: TC1, DH1; MFG7: TC1, DH1) due to full surface conductivity at 85 °C is approximately 79.4 %. In comparison, the average power drop due to humidity is approximately 22.1% [6].

The average power drop due to full surface conductivity at both temperatures (85 °C and 60 °C) for the six modules (MFG5: TC2, DH2; MFG7: TC1, TC2, DH1, DH2) is approximately 72.4 %. The full carbon condition has a very adverse effect on the modules and it does not appear to simulate the naturally occurring humidity condition where the surface conductivity is very limited and interfacial conductivity (glass/encapsulant; cell/encapsulant; encapsulant/backsheet) could also occur. Therefore, it is recommended to utilize the humidity based surface conductivity method rather than carbon (or any metallic layer) based surface conductivity method.

Figure 4.7 shows the remaining power of all the modules tested in this thesis work.

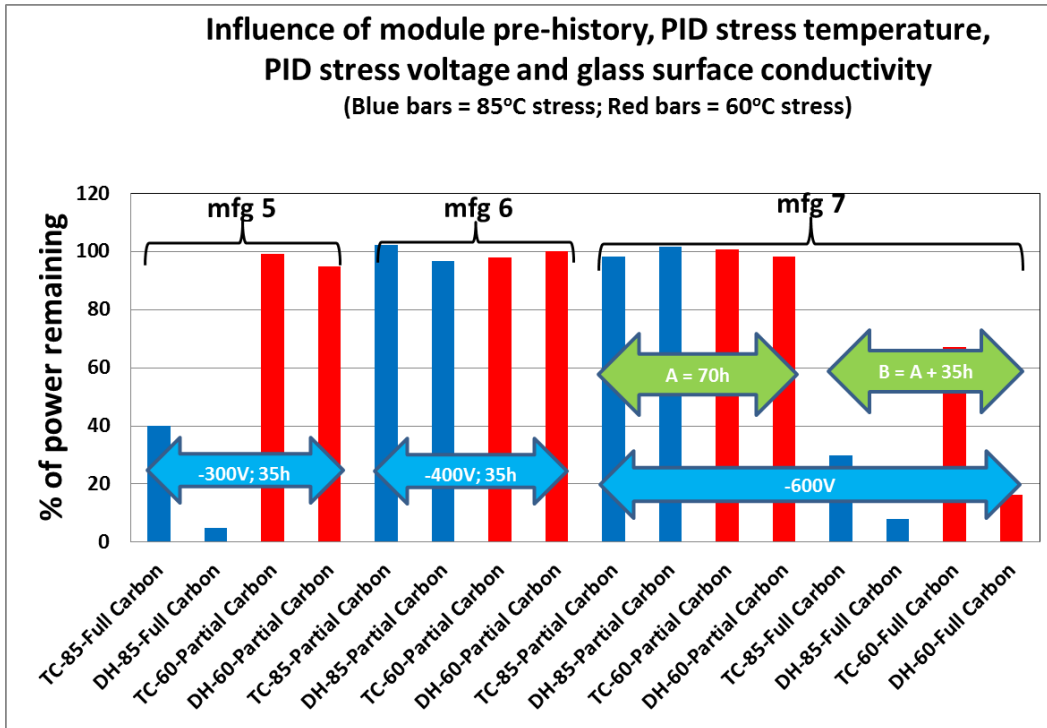


Figure 4.7: Performance degradation due to PID for all the modules.

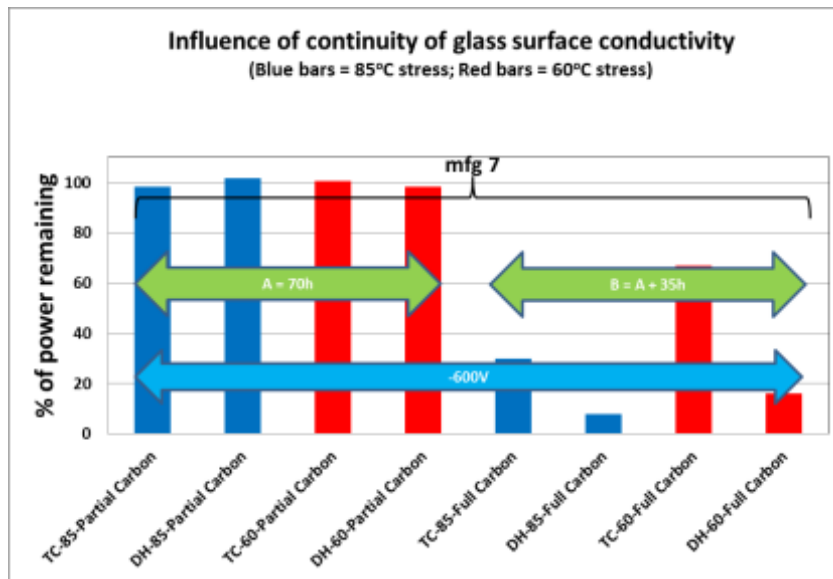


Figure 4.8: Influence of continuity of glass surface conductivity on PID

Figure 4.8 depicts the percent of power remaining for modules that underwent PID under the partial carbon condition and then under the full carbon condition. From the above, it is evident that degradation is negligible/ non-existent under the partial carbon condition, while it is detrimental in full carbon condition. Since, surface conductivity is the predominant conductive path [6], disrupting it drastically reduces or eliminates the PID effect. Therefore, applying a 2 cm wide layer of water repellent (e.g. Teflon) on the edges of module is expected to either prevent or drastically reduce PID from occurring.

In the previous studies, the performance of the modules was found to have degraded significantly at the negative bias when the surface conductivity was existing (either through carbon layer extending to the frame or humidity). When the surface continuity in this current study was disrupted by maintaining a 2 cm gap from the frame to the edge of the conductive layer, the degradation was found to be absent or negligibly small, even after 35 hours under negative bias and at elevated temperatures. This preliminary study appears to indicate that if the continuity of the glass surface conductivity is disrupted at the inside boundary of the frame, the modules could become immune to PID losses. Previous studies by other research groups indicated that the PID losses can be contained either by modifying the anti-reflection coating of the cells or the encapsulant bulk resistivity. This preliminary study indicates the PID losses could be contained by disrupting the surface conductivity of the glass at the inside boundary of the frame. The surface conductivity of the glass due to water layer formation under humid conditions could be disrupted by the following methods; applying a water

repelling (hydrophobic) close to the frame such as a highly transmittance surface coating (such as Teflon) or modifying the frame/glass edges with water repellent properties. The finding of this preliminary study is recommended to be extended with a larger number of test samples from a larger number of manufacturers so the surface conductivity disruption effect on PID can be fully analyzed and understood.

The full carbon coated results shown in Figures 4.7 and 4.8 also indicate the following:

- The DH stressed modules seem to undergo higher PID losses as compared the TC stressed modules, and this result is consistent with previous findings [6]. The 85°C temperature condition for the PID evaluation seems to be very aggressive as compared to the 60°C temperature condition. The 85°C temperature condition with fully covered metallic conductive surface may not be simulating the actual field failure mechanism related to PID.

#### 4.4 Determination of Activation Energy

Activation energy is defined as the minimum amount of energy required to initiate a reaction. The higher the temperature, the faster the reaction will occur. While the temperature increases, the electron collision rate within the interfaces accelerates and results in a higher kinetic energy which will affect the activation energy. The rate of the PV module deterioration can potentially be predicted by using the Arrhenius equation. In general, Arrhenius plots are used to analyze the effect of temperature on the rates of chemical reactions. The Arrhenius equation

can explain the rate of reaction depending on the temperature that the sample is tested [6].The governing Arrhenius equation is-

$$r = A \times \exp\left(-\frac{E_a}{k \times T}\right)$$

r- Rate of failure

A- Proportional constant

E<sub>a</sub>- Activation energy (eV)

T- Absolute temperature (°K)

k- Stefan-Boltzmann constant =  $8.6 \times 10^{-5}$  (eV/K)

Using the module failure rates at high temperatures and the Arrhenius equation we can predict the reaction rates at lower temperatures by extrapolating the Arrhenius curve [5].

Figure 4.11 shows the Arrhenius plots for the first five hours of modules TC 1 and DH 1 under full carbon condition.

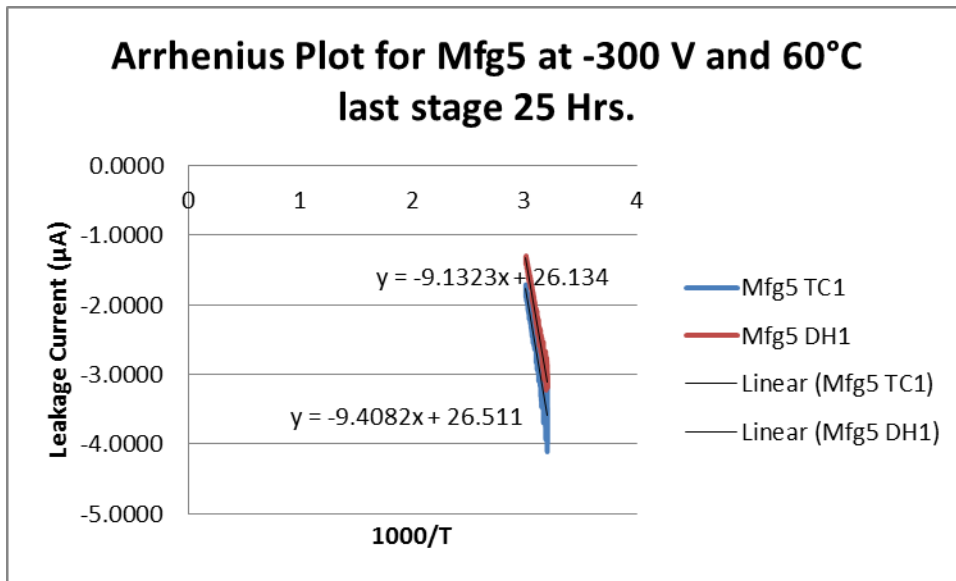


Figure 4.9: Arrhenius plot for Mfg 5 during first 5 hours of PID stress.

Table 4.5 provides the activation energy of the modules during 5 hours, 10 hours and 35 hours at -300V stress voltage. During the first 5 hours, the modules were stressed under the full carbon condition, whereas, they were stressed under partial carbon condition for the rest of the test. This is evident in a higher activation energy during first 5 hours, than the second.

Table 4.5: Activation energies of modules stressed at -300 V and 85 °C. Note that, for the first 5 hours, the modules were stressed under full carbon condition.

<b>Module</b>	<b>PID Stress Temperature (°C)</b>	<b>After 5hr PID (Full Carbon) (eV)</b>	<b>After 10hrs PID (Partial Carbon) (eV)</b>	<b>After 35hrs PID (Partial Carbon) (eV)</b>
TC 1	85	0.58	0.86	0.86
DH 1	85	0.60	0.81	0.86
<b>Module</b>	<b>PID Stress Temperature (°C)</b>	<b>After 5hr PID (Partial Carbon) (eV)</b>	<b>After 10hrs PID (Partial Carbon) (eV)</b>	<b>After 35hrs PID (Partial Carbon) (eV)</b>
TC 2	60	0.36	0.62	0.79
DH 2	60	0.44	0.81	0.81

#### 4.5 Charge Transferred

Due to the leakage current over the test period, a charge is transferred. The following formula gives us the charge transferred to the module.

$$C = I \times t$$

Where

C- Charge transferred

I- Sum of the leakage current over test period



T- Test time

Table 4.6: Charge (Coulombs) transferred.

<b>Module</b>	<b>0-5hrs (full carbon) (Coulomb)</b>	<b>5-10hrs (partial carbon) (Coulomb)</b>	<b>10-35hrs (partial carbon) (Coulomb)</b>
TC 1	0.130	0.068	0.097
DH 1	0.445	0.101	0.180
<b>Module</b>	<b>0-5hrs (partial carbon) (Coulomb)</b>	<b>5-10hrs (partial carbon) (Coulomb)</b>	<b>10-35hrs (partial carbon) (Coulomb)</b>
TC 2	0.005	NA	0.018
DH 2	0.002	NA	0.028

From the table 4.6 above, it can be concluded that the charge transferred is high due to the carbon paste touching the frame and increasing the conductivity multiple folds.

#### 4.6 Potential Induced Recovery

After stressing the modules for a cumulative time of 105 hours, the modules were stressed under positive (+) bias for 35 more hours to recover their lost power. The following table shows the parameters used for recovering the modules. In addition, full carbon condition was used during recovery.

Table 4.7: Test parameters during recovery for Mfg7 under full carbon condition.

<b>Manufacturer 7</b>		
<b>Parameter</b>	<b>Group1</b>	<b>Group2</b>
Voltage	+600 V	+600 V
Temperature	85 °C	60 °C
Relative Humidity	0-5 %	0-5 %
Time	35 Hrs.	35 Hrs.

Table 4.8: Power recovered after recovery test for manufacturer 7.

<b>Manufacturer 7</b>					
<b>Module</b>	<b>Temperature (°C)</b>	<b>After PID (W)</b>	<b>% Remaining</b>	<b>PID After (W)</b>	<b>% Remaining</b>
<b>TC 1</b>	85	60.49	29.96	94.9	46.95
<b>DH 1</b>	85	14.21	7.92	22.43	12.54
<b>TC 2</b>	60	129.18	67.02	183.55	95.61
<b>DH 2</b>	60	26.78	16.15	54.6	34.83

Table 4.10 shows the power recovered by the modules after recovery testing. It can be seen that the modules have recovered a significant amount of power after only 35 hours of recovery. Further recovery testing may enhance the power recovered.

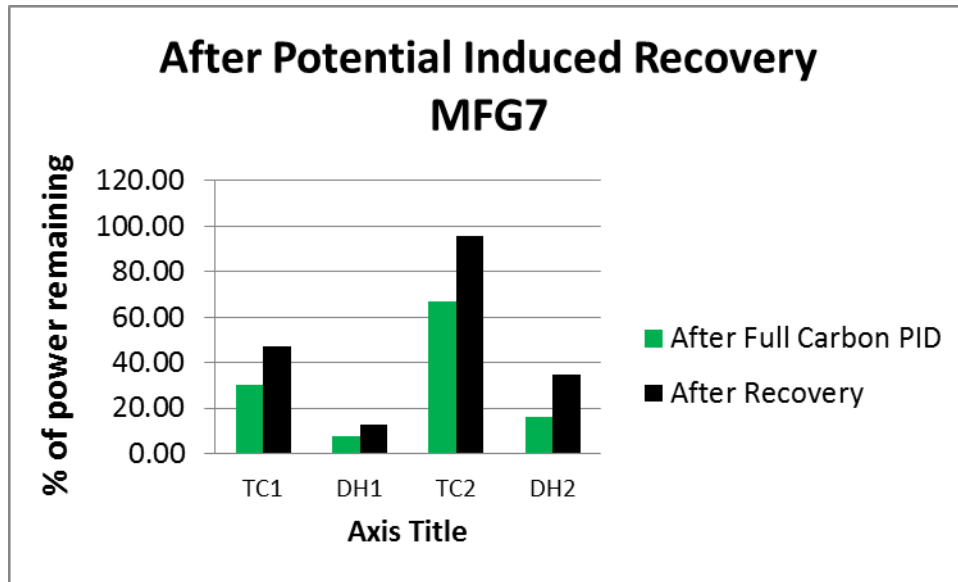


Figure 4.10: Performance comparison before and after potential induced recovery.

#### 4.7 Calculation of Series Resistance ( $R_s$ )

Using the single slope method, a single light I-V curve at an irradiance of 1000W/m<sup>2</sup> was collected to determine  $R_s$  value. By selecting 30 data points close to the open circuit voltage ( $V_{oc}$ ) of an IV curve, and obtaining a linear fit to the extracted data,  $R_s$  is calculated as inverse of slope of the linear curve.

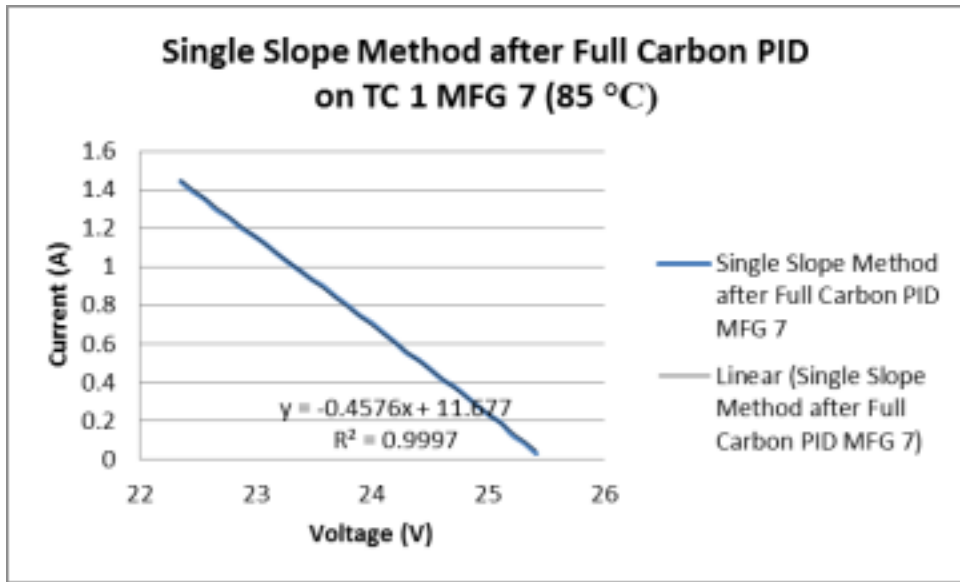


Figure 4.11: Calculating  $R_s$  of TC1 MFG7 module after full carbon PID by single slope method.

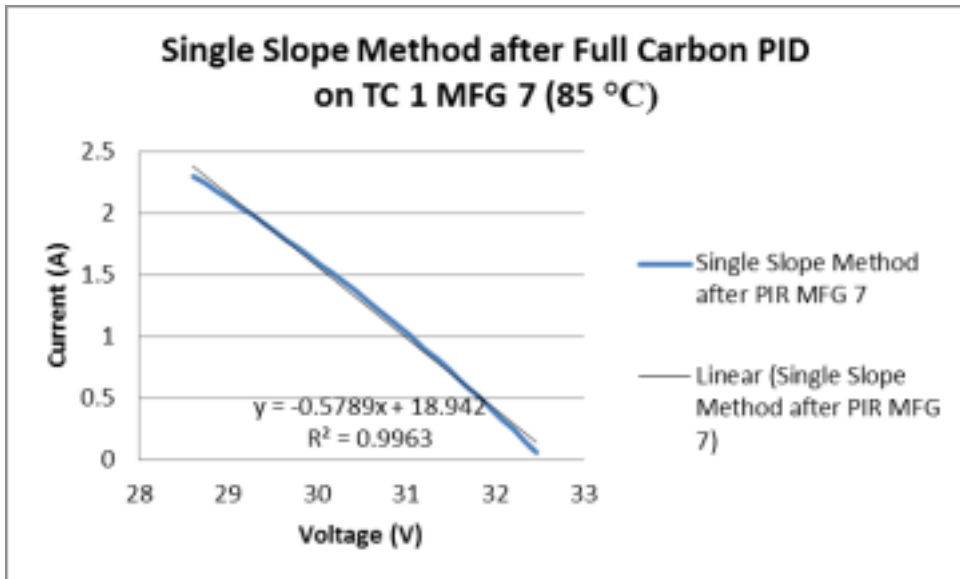


Figure 4.12: Calculating  $R_s$  of TC1 MFG7 module after PIR by single slope method.

The two plots above shows I-V curves before full carbon PID and post-PIR. The series resistance is the inverse of the slope of the curve, which for the

above value are 2.19  $\Omega$  and 1.72  $\Omega$ . The following table consists of  $R_S$  values of MFG7 modules.

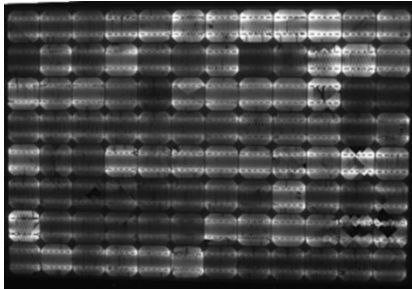
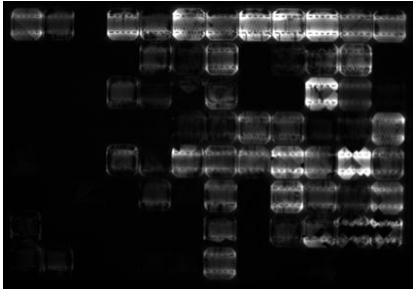
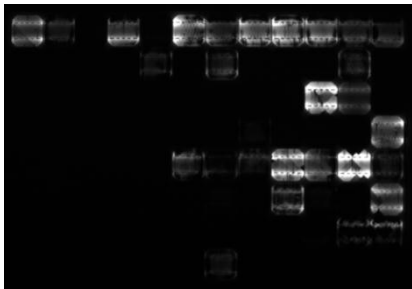
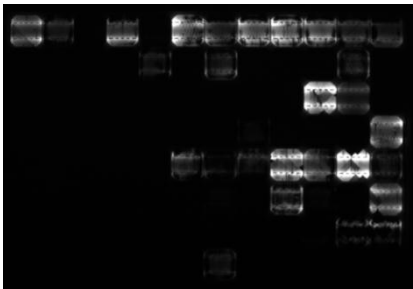
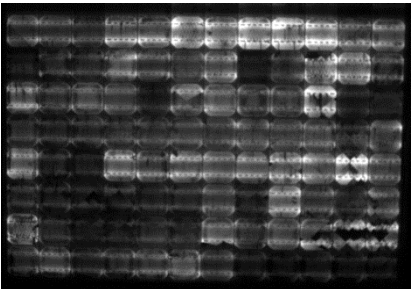
Table 4.9: Series resistance values for MFG 7 modules.

	<b><math>R_S</math> After PID</b>	<b><math>R_S</math> After PIR</b>
<b>TC1</b>	2.10	1.73
<b>DH1</b>	1.12	1.29
<b>TC2</b>	2.19	1.73
<b>DH2</b>	1.22	1.46

#### 4.7 Image Characterization

As described in Chapter 3, a visual inspection was performed on every module, followed by electro-luminescent (EL) imaging and infra-red (IR) imaging. Table 4.12 consists of EL images of TC1 (mfg5) module before, during & after PID and after recovery. These modules were stressed in the full carbon condition for the first 5 hours of PID and then under the partial carbon condition. The module degradation is clearly visible, with no current being produced by the dark areas. From this, we can conclude that most of the degradation occurred during 5 hours of PID full carbon condition. Also, the EL images show us that the DH modules are more susceptible to PID than TC modules.

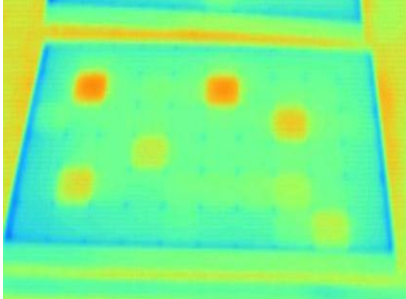
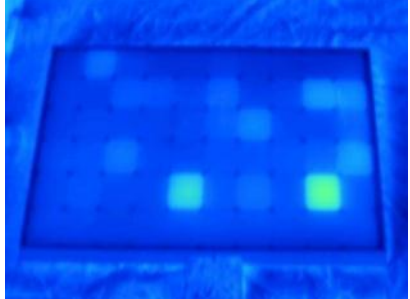
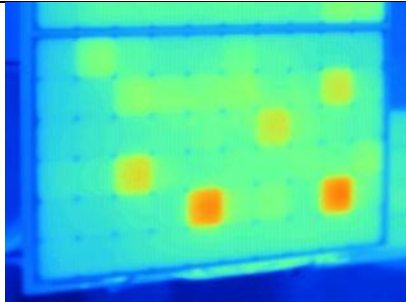
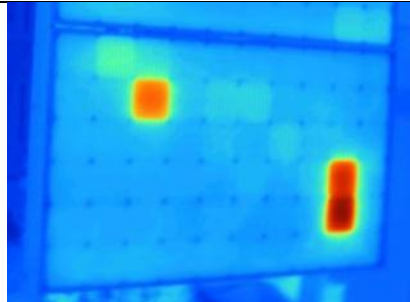
Table 4.10: Electro-luminescence images of a TC1 module (mfg5).

Pre-PID Stressed	5 hrs. into PID (Full Carbon)
	
10 hrs. into PID (Partial Carbon)	35 hrs. into PID (Partial Carbon)
	
35 hrs. into PIR (Full Carbon)	
	

From the following IR images (Table 4.13) of a DH module, it is observed that the module post recovery has three extreme hot spots which are about 35 °C to 40 °C hotter than the rest of the module. In addition there were three other hot

spots which were about 20 °C higher than their surroundings cells. This may allude to some mechanism where the module degraded during the recovery process.

Table 4.11: Infrared images of a DH1 module (mfg6)

Before PID	After 10 Hrs. of PID (Partial Carbon)
	
After 35 Hrs. of PID (Partial Carbon)	After 35 Hrs. of PIR (Full Carbon)
	

#### 4.8 Summary of PID Evaluations at ASU-PRL

The PID study performed so far at ASU-PRL is summarized in this section.

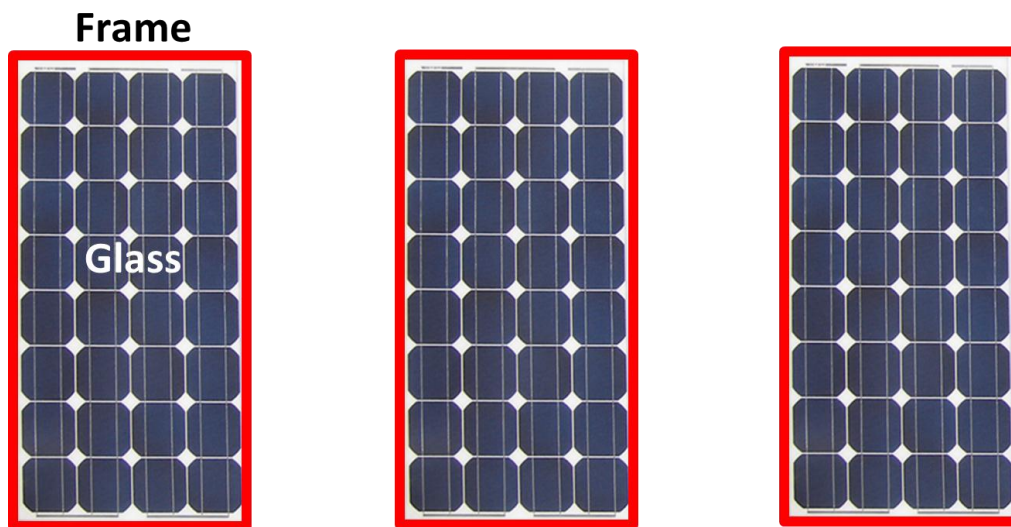
PID effect of c-Si modules can be reduced or eliminated by:

- 1) By modifying AR coating of the cells

- 2) By increasing the bulk conductivity of encapsulant
- 3) By disrupting the glass surface conductivity

The influence of surface conductivity, including the conductivity disruption, of the glass on PID is presented below. Figure 4.13 shows the PV modules with no surface conductive layers. Figure 4.14 shows the PV modules with high surface conductive layer of carbon (Figure 4.14A), low surface conductive layer of water (Figure 4.14B), disrupted conductive layer of water (Figure 4.14C) and disrupted conductive layer of carbon (Figure 4.14D). Figure 4.14D simulates the disrupted conductivity of glass surface due to the absence of water layer near the frame. The absence of water layer near the frame may be achieved by using a hydrophobic layer near the frame or by treating the glass surface near the frame for hydrophobicity. The objective of this work is to investigate if the PID effect can be decreased or eliminated by disrupting the glass surface conductivity near the frame edges.





**Modules with no surface conductive layers**

Figure 4.13: PV modules with no surface conductive layers

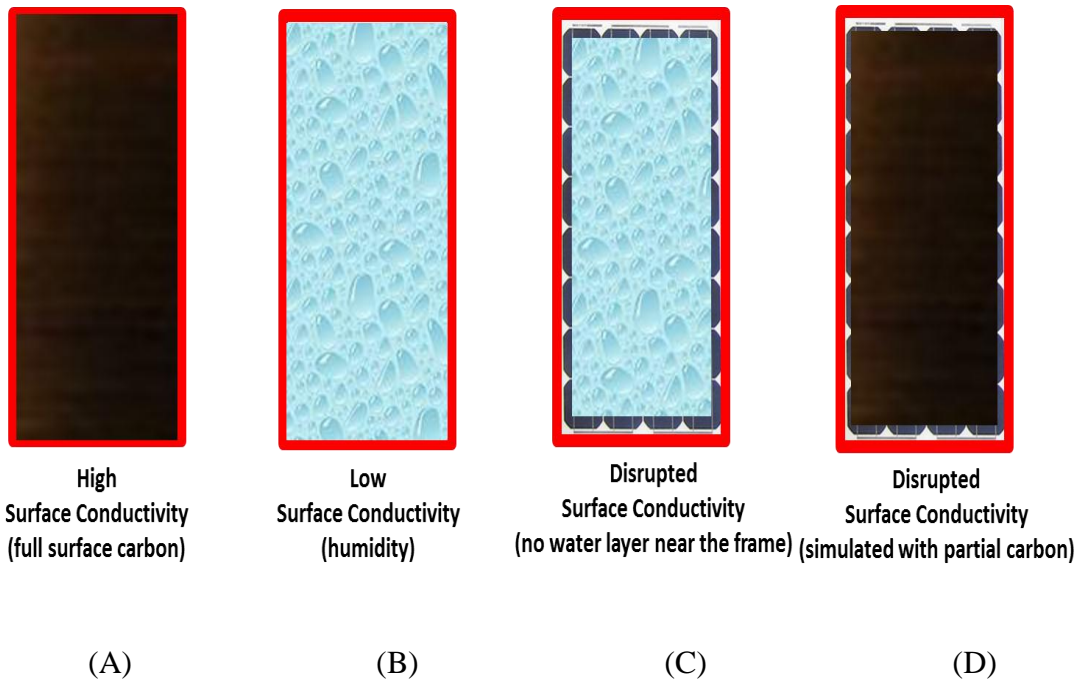


Figure 4.14: Surface conductivity of glass with full surface carbon for high surface conductivity (A), with humidity for low surface conductivity (B), with no water layer near the frame for disrupted conductivity (C) and with no carbon layer near the frame for disrupted conductivity (D).  
figure 4.14D simulates Figure 4.14C condition.

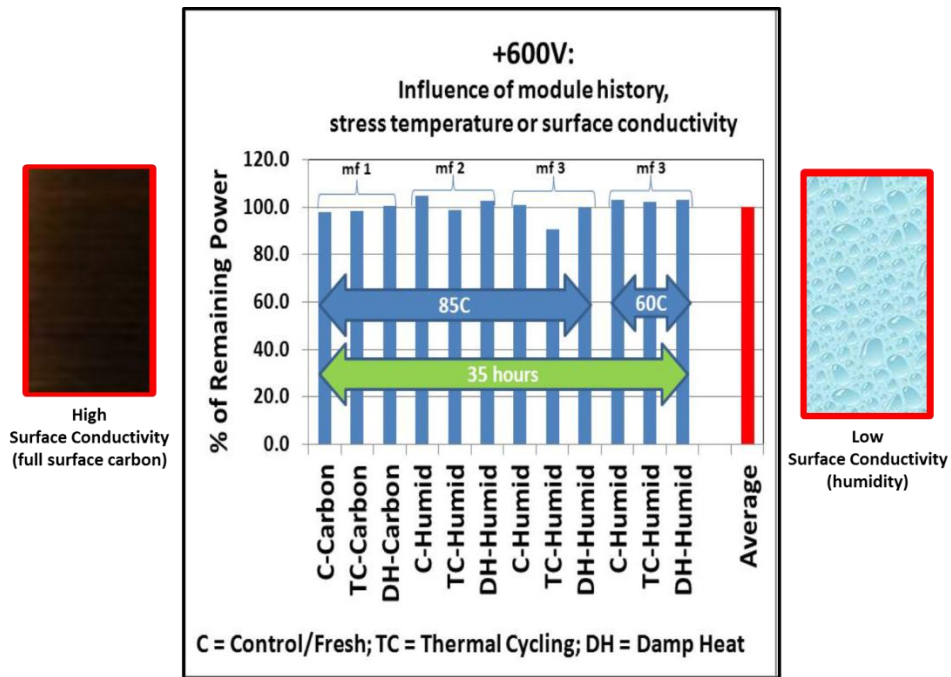


Figure 4. 15: +600V: Influence of module history, stress temperature or surface conductivity [26]

Figure 4.15 compares the percentage of power remaining in the modules after a +bias stress. Mfg1 modules were stressed under the full carbon (high conductivity) condition, while the mfg2 and mfg3 were stressed under low surface conductivity (85% RH). The modules under + bias had [26]:

- No PID effect irrespective of history of modules
- No PID effect irrespective of level (high or low) of surface conductivity
- No PID effect irrespective of manufacturer

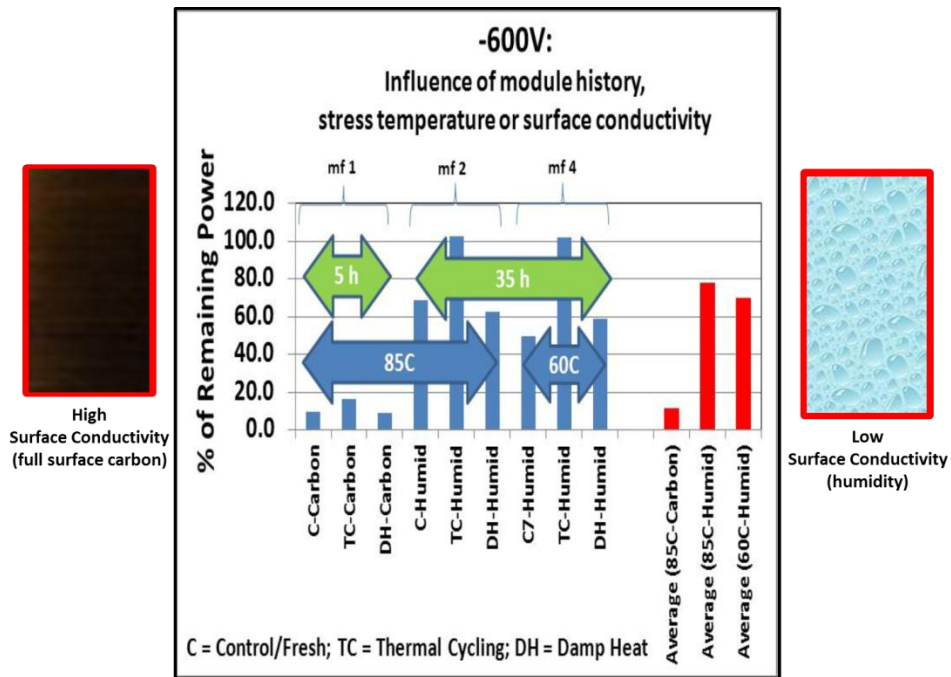


Figure 4.16: -600V: Influence of module history, stress temperature or surface conductivity [26].

Figure 4.16 compares the percentage of power remaining in the modules after they underwent PID under –bias.

The modules under negative bias had [5] [6]:

- The PID effect depending on the history of modules
- The PID effect depending on the level (high or low) of surface conductivity
- The PID effect depending on the manufacturer

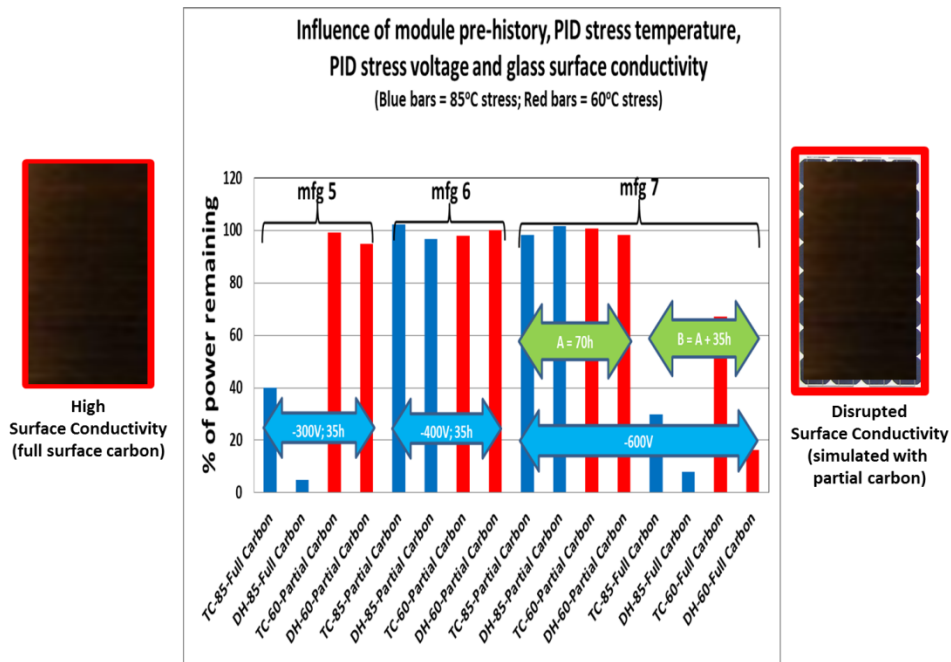


Figure 4.17: Influence of module history, PID stress temperature and glass surface conductivity.

Figure 4.17 compares the percentage of power remaining in the modules after they underwent PID under negative bias.

The test results modules under negative bias with disrupted surface conductivity seem to indicate [this thesis work]:

- No PID effect irrespective of history of modules
- No PID effect irrespective of PID stress temperature
- No PID effect irrespective of manufacturer

## CHAPTER 5

### CONCLUSIONS

In this study, the PV modules from three different manufacturers were investigated for the potential induced degradation. The following key conclusions may be obtained:

- Influence of glass surface conductivity: Irrespective of history, PID stress temperature or PID stress voltage, the average drop due to full carbon surface conductivity is 73% and due to partial carbon conductivity is only less than 1%.
- Influence of pre-history: Irrespective of PID stress temperature or PID stress voltage, the average drop due to damp heat pre-history is about 2% and due to thermal cycling pre-history is about 0% when the surface conductivity is disrupted.
- Influence of PID stress temperature: Irrespective of pre-history or PID stress voltage, the average drop due to 60°C and 85°C PID stress when the surface conductivity is disrupted is zero or negligibly small.

Some other conclusions that could be made from this research and previous works conducted at ASU-PRL are:

- Under a positive voltage bias, no degradation was observed for hot-dry climatic conditions.
- Under a negative voltage bias, significant degradation was observed.

- Under high-surface conductivity, higher degradation was observed.
- Failure mechanism under negative voltage bias appears to be mostly or fully reversible by applying a positive voltage.

The following are a few suggestions that might be useful during future studies.

- All samples should be from the same manufacturer and of same model.
- Due to various factors, dark IV could not be obtained until the final stages of testing. Having dark IVs would greatly help in the calculation of the series resistance.

Further studies could be made on

- Optimum width of the moisture repellent/ conductivity disrupting layer.
- Why TC modules are developing higher resistance to PID?
- Increasing stress voltage to 1500 V.
- Increasing the stress time.
- Increasing number of samples.

## REFERENCES

- [1] R. G. Ross, "Crystalline-silicon, reliability lessons for thin-film modules," in *18th IEEE Photovoltaic Specialists Conference (PVSC)*, Las Vegas, NV, 1985.
- [2] "Bath tub curve," [Online]. Available: [http://en.wikipedia.org/wiki/Bathtub\\_curve](http://en.wikipedia.org/wiki/Bathtub_curve).
- [3] G. Mon and R. G. Ross, "Effects of temperature and moisture on module leakage currents," in *18th IEEE Photovoltaic Specialists Conference (PVSC)*, Las Vegas, NV, 1985.
- [4] Pingel, S; Frank, O; Winkler, M; Dyran, S; Geipel, T; Hoehne, H; Berghold, J,; "Potential Induced Degradation of Solar Cells and Panels," in *35th IEEE Photovoltaic Specialists Conference (PVSC)*, Honolulu, HI, 2010.
- [5] S. Goranti, "Potential Induced Degradation (PID) of Accelerated Stressed Photovoltaic Modules," 2011.
- [6] F. Ebneali, "Potential Induced Degradation of PV Modules: Influence of Temperature and Surface Conductivity," 2012.
- [7] R. H. Bube, *Photovoltaic Materials*, Imperial College Press, 1998.
- [8] S. Fonash, *Solar Cell Device Physics*, Academic Press, 2010, p. 1.
- [9] "What is accelerated life testing?," [Online]. Available: [http://www.weibull.com/AccelTestWeb/what\\_is\\_accelerated\\_life\\_testing\\_.htm](http://www.weibull.com/AccelTestWeb/what_is_accelerated_life_testing_.htm). [Accessed 18 November 2011].
- [10] "Types of Accelerated Tests," [Online]. Available: [http://www.weibull.com/AccelTestWeb/types\\_of\\_accelerated\\_tests.htm](http://www.weibull.com/AccelTestWeb/types_of_accelerated_tests.htm). [Accessed 18 November 2011].



- [11] M. L. Morelli, "Effectiveness of HALT and HASS," 2006. [Online]. Available: <http://www.acteq.fr/biblio/effectiveness-of-halt-and-hass.pdf>.
- [12] J. H. Wohlgemuth and M. D. Frederick, "Reliability Testing of PV Modules," in *Photovoltaic Energy Conversion, 1994.*, Waikoloa, HI, 1994.
- [13] International Electrotechnical Commission (IEC) standard, IEC 61215, 2.0 ed., International Electrotechnical Commission, 2005.
- [14] J. A. del Cueto and S. R. Rummel, "Degradation of Photovoltaic Modules Under High Voltage Stress in the Field," in *Reliability of Photovoltaic Cells, Modules, Components, and Systems III: SPIE Conference*, San Diego, CA, 2010.
- [15] P. Hacke, S. Glick, S. Johnston, R. Reedy, J. Pankow, T. Kent and S. Kurtz, "Influence of Impurities in Module Packaging on Potential-Induced Degradation," in *22nd Workshop on Crystalline Silicon Solar Cells & Modules: Materials and Processes*, Vail, Colorado, 2012.
- [16] P. Hacke, M. Kempe, K. Terwilliger, S. Glick, N. Call, S. Johnston, S. Kurtz, I. Bennett and M. Kloos, "Characterization of Multicrystalline Silicon Modules with System Bias Voltage Applied in Damp Heat," in *25th European Photovoltaic Solar Energy Conference and Exhibition (EUPVSEC)*, Valencia, 2010.
- [17] V. Naumann, C. Hagendorf, S. Grosser, M. Werner and J. Baghdan, "Micro Structural Root Cause Analysis of Potential Induced," in *2nd International Conference on Crystalline Silicon Photovoltaics*, 2012.
- [18] K. Morita and O. Kiyoki, "Novel Selective Etching Method for Silicon Nitride Films on Silicon Substrates by Means of Subcritical Water," *Ind. Eng. Chem. Res.*, vol. 39, no. 12, p. 4684-4688, 28 October 2000.
- [19] J. Singh, "Investigation of 1,900 individual field aged photovoltaic modules for potential induced degradation (PID) in a positive biased power plant," 2011.

- [20] C. Honsberg and S. Bowden, "Electroluminescence," [Online]. Available: <http://pveducation.org/pvcdrom/characterisation/electroluminescence>. [Accessed August 2011].
- [21] C. Honsberg and S. Bowden, "IV Curve," [Online]. Available: <http://www.pveducation.org/pvcdrom/solar-cell-operation/iv-curve>.
- [22] "Description," [Online]. Available: <http://www.daystarpv.com/curvetracer2.html>.
- [23] "2700 Datalogger," [Online]. Available: <http://www.keithley.com/data?asset=51943>.
- [24] "Keithley 2700 DMM," [Online]. Available: <http://www.keithley.com/products/data/datalogger/?mn=2700>.
- [25] "PID Test System, Instruction Manual, ASU Photovoltaic Reliability Laboratory," 2011.
- [26] G. Tamizhmani, "Potential Induced Degradation: Analysis of 1900 Individual Modules," in *2012 (PVMRW)*, Golden, CO, 2012.
- [27] "Carbon Conductive Grease 846," [Online]. Available: <http://www.mgchemicals.com/products/846.html>. [Accessed November 2011].
- [28] International Electrotechnical Commission (IEC) standard, IEC 60904 Part 1, International Electrotechnical Commission, 1987.
- [29] International Electrotechnical Commission (IEC) standard, IEC 60904 Photovoltaic devices - Part 2, IEC, 1989.

APPENDIX A

[POTENTIAL INDUCED DEGRADATION]

DATA COLLECTED AUGUST 2011–APRIL 2012

Table A 1: Performance measurement of manufacturer 5 during PID testing.

Temperature (°C)	Voltage (V)	Condition	Time (Hrs.)		Before (W)	After (W)	Remaining (%)
85	-300	Full Carbon (0-5 h)	35	TC1	201.57	80.41	39.89
				DH1	186.08	8.78	4.72
60		Partial Carbon	35	TC2	226.98	225.36	99.29
				DH2	192.49	182.77	94.95

71

Table A 2: Performance measurement of manufacturer 6 during PID testing under partial carbon condition

Temperature (°C)	Voltage (V)	Condition	Time (Hrs.)		Before (W)	After (W)	Remaining (%)
85	-400	Partial Carbon	35	TC1	193.95	198.36	102.27
				DH1	205.83	199.48	96.91
60		Partial Carbon	35	TC2	197.57	193.63	98.01
				DH2	179.99	180.22	100.13

Table A 3: Performance measurement of manufacturer 7 during 35 Hrs. of partial carbon PID testing.

Temperature (°C)	Voltage (V)	Condition	Time (Hrs.)		Before (W)	After (W)	Remaining (%)
85	-600	Partial Carbon	35	TC1	205.3	201.9	98.3
				DH1	176.4	179.4	101.7
60		Partial carbon	35	TC2	191.6	192.8	100.6
				DH2	168.7	165.8	98.3

72

Table A 4: Performance measurement of manufacturer 7 during 35 Hrs. of full carbon PID testing.

Temperature (°C)	Voltage (V)	Condition	Time (Hrs.)		Before (W)	After (W)	Remaining (%)
85	-600	Full carbon	35	TC1	201.9	60.5	30.0
				DH1	179.4	14.2	7.9
60		Full carbon	35	TC2	192.8	129.2	67.0
				DH2	165.8	26.8	16.2

APPENDIX B

[POTENTIAL INDUCED RECOVERY]

DATA COLLECTED JANUARY-APRIL 2012

Table B 1: Comparison of performance of Mfg 5 modules before and after recovery.

Temperature (°C)	Voltage (V)	Condition	Time (Hrs.)		Before (W)	After (W)	Remaining (%)
85	+300	Full carbon	35	TC1	80.41	185.92	92.24
				DH1	8.78	115.45	62.04
60		Full carbon	35	TC2	225.36	219.94	96.90
				DH2	182.77	182.34	94.73

Table B 2: Comparison of performance of Mfg 6 modules before and after recovery.

Temperature (°C)	Voltage (V)	Condition	Time (Hrs.)		Before (W)	After (W)	Remaining (%)
85	+400	Full carbon	35	TC1	198.36	102.27	188.62
				DH1	199.48	96.91	191.55
60		Full carbon	35	TC2	193.63	98.01	199.72
				DH2	180.22	100.13	182.54

Table B 3: Comparison of performance of Mfg 7 modules before and after recovery.

Temperature (°C)	Voltage (V)	Condition	Time (Hrs.)		Before (W)	After (W)	Remaining (%)
85	+600	Full carbon	35	TC1	60.49	29.96	94.9
				DH1	14.21	7.92	22.43
60		Full carbon	35	TC2	129.18	67.02	183.55
				DH2	26.78	16.15	54.6



APPENDIX C

[LEAKAGE CURRENT VS. TIME]

DATA COLLECTED DECEMBER 2011-APRIL 2012

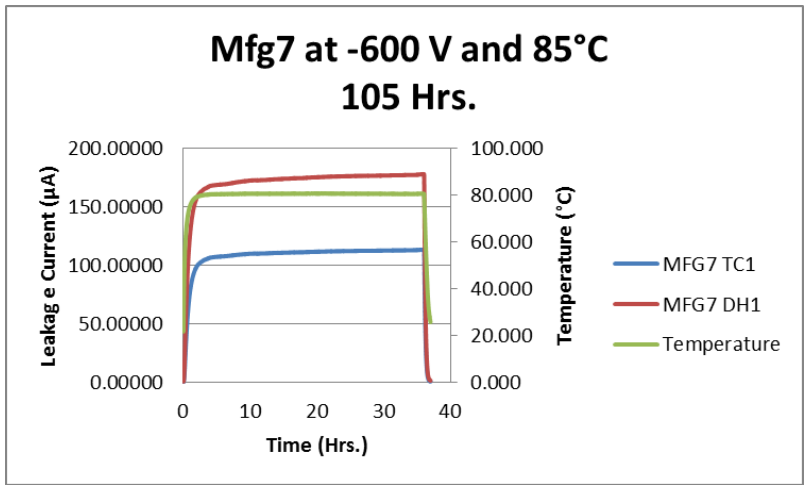


Figure C 1 Leakage current (µA) versus time (Hrs.) for TC1 and DH1 (Mfg7) during third stage (35 hours of PID under full carbon condition).

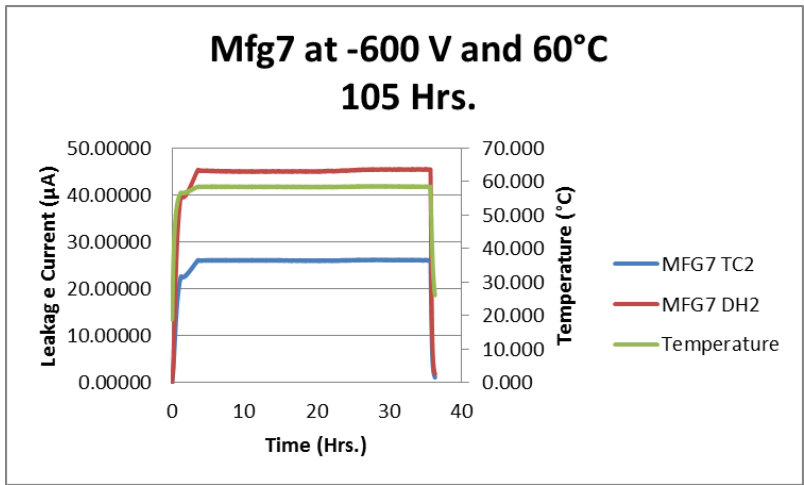


Figure C 2 Leakage current (µA) versus time (Hrs.) for TC2 and DH2 (Mfg7) during third stage (35 hours of PID under full carbon condition).

APPENDIX D

[ARRHENIUS PLOTS]

DATA COLLECTED DECEMBER 2011-APRIL 2012

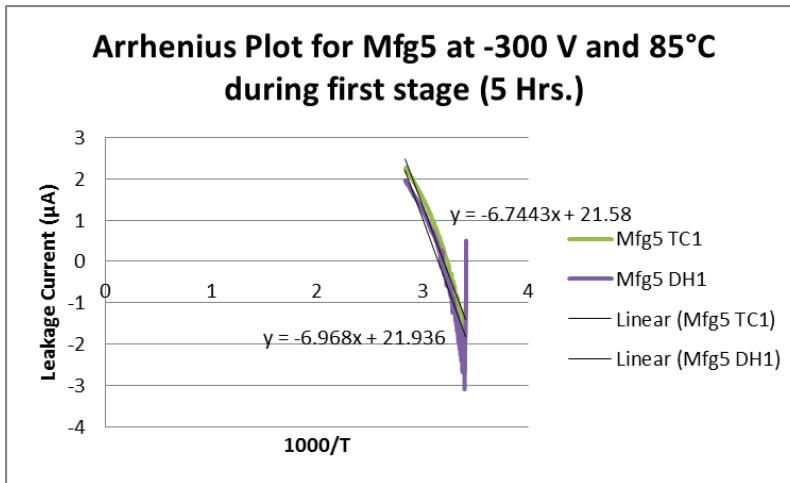


Figure D 1 Arrhenius plot for TC1 and DH1 (Mfg 5) during first stage (5 hours of PID).

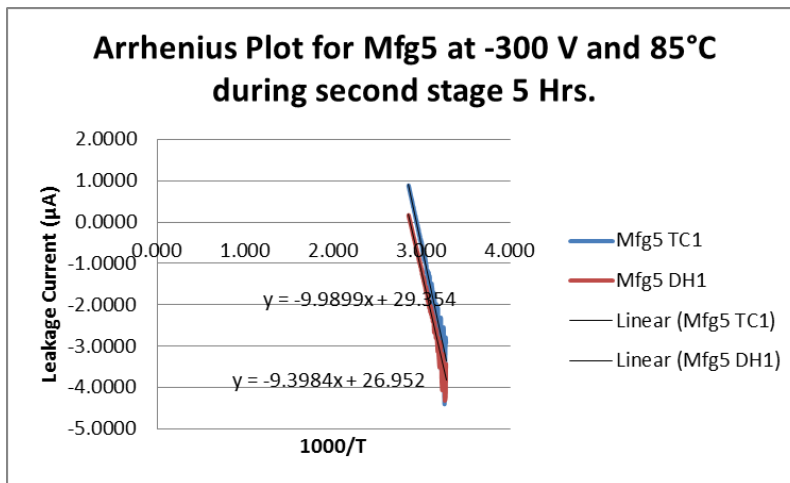


Figure D 2: Arrhenius plot for TC1 and DH1 (Mfg 5) during second stage (5 hours of PID).

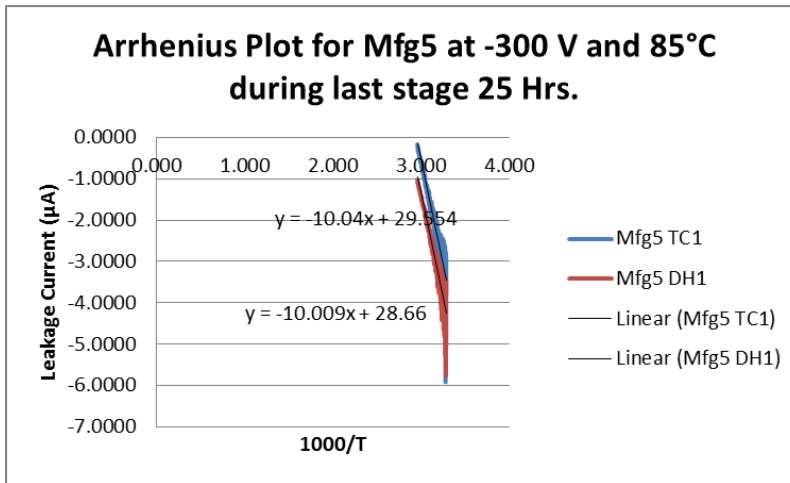


Figure D 3 Arrhenius plot for TC1 and DH1 (Mfg 5) during third stage (25 hours of PID).

APPENDIX E

[DARK IV PLOTS]

DATA COLLECTED JANUARY 2012-APRIL 2012

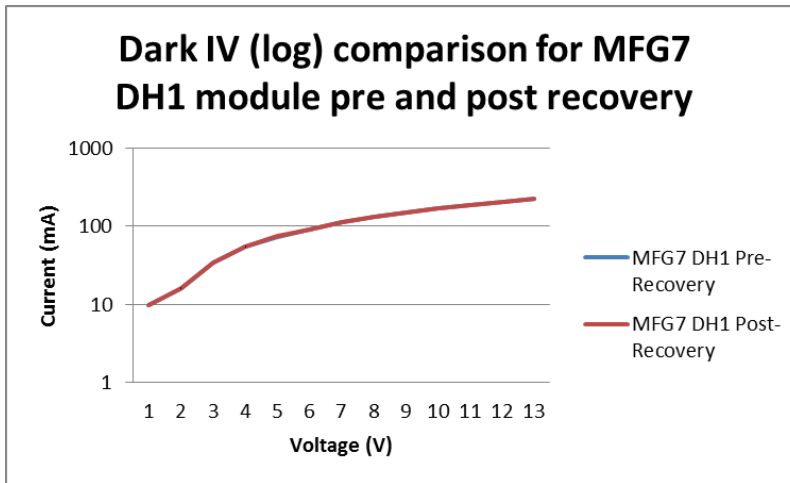


Figure E 1 Pre and post-recovery dark IVs (log scale) comparison for MFG7 DH1 module.

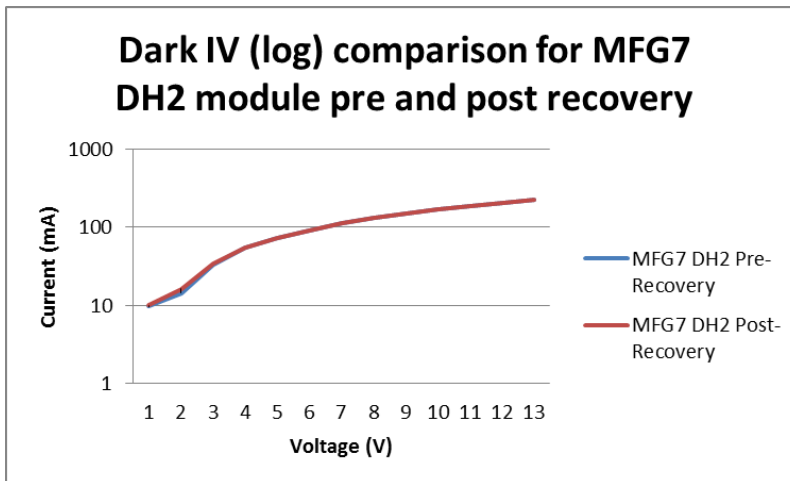


Figure E 2 Pre and post-recovery dark IVs (log scale) comparison for MFG5 DH2 module.

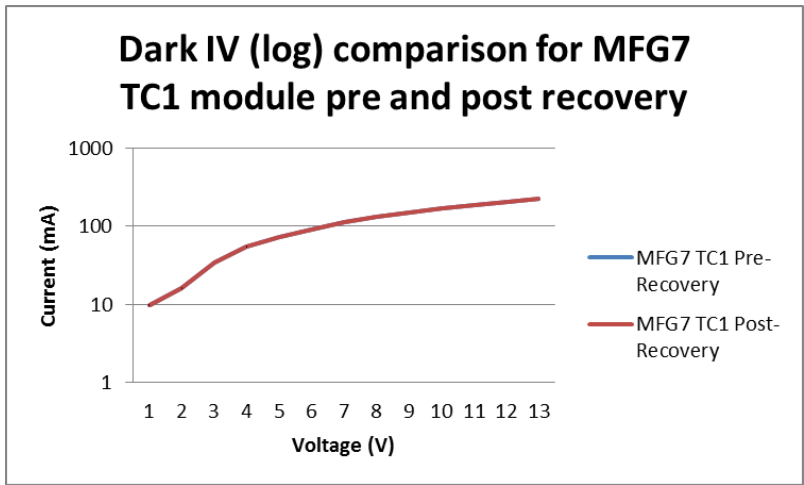


Figure E 3 Pre and post-recovery dark IVs (log scale) comparison for MFG7 TC1 module.

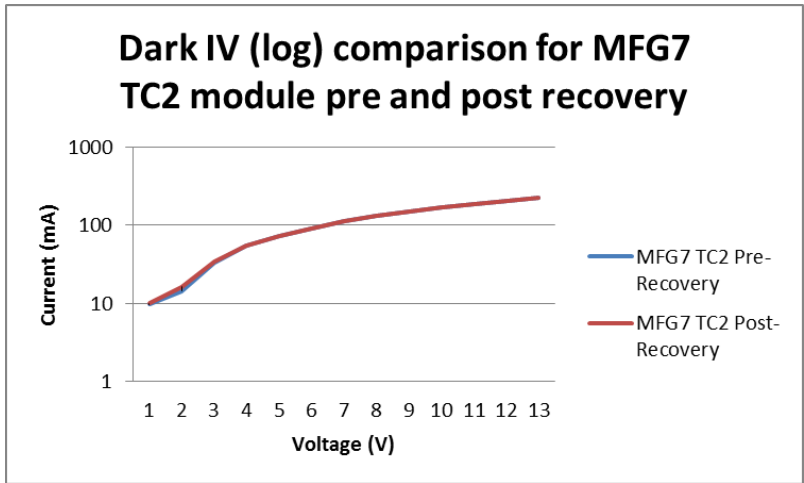


Figure E 4 Pre and post-recovery dark IVs (log scale) comparison for MFG7 TC2 module.

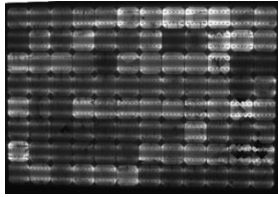
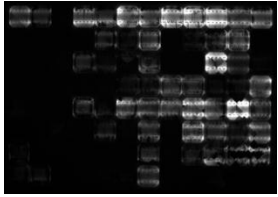
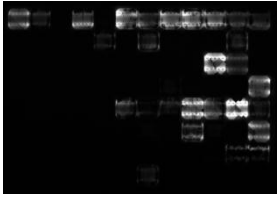
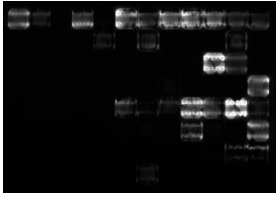
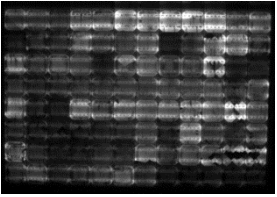


APPENDIX F

[ELECTRO-LUMINESCENCE IMAGING]

DATA COLLECTED AUGUST 2011-APRIL 2012

Table F 1: EL images of the MFG5 DH1 module through various test stages.

Pre-PID Stressed	5 Hrs. into PID(Full Carbon)	10 Hrs. into PID (Partial Carbon)	35 Hrs. into PID(Partial Carbon)	35 Hrs. into PIR (Full Carbon)
				

85

Table F 2: EL images of the MFG5 TC1 module through various test stages.

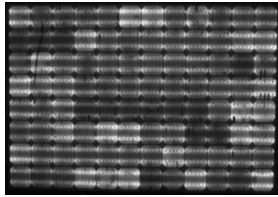
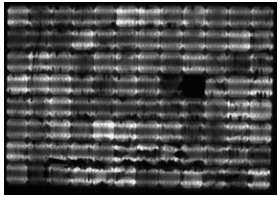
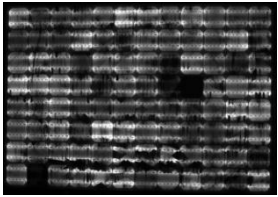
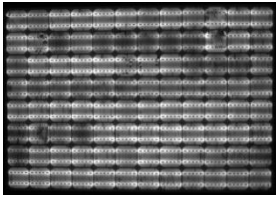
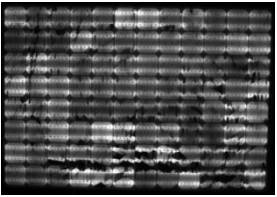
Pre-PID Stressed	5 Hrs. into PID (Full Carbon)	10 Hrs. into PID (Partial Carbon)	35 Hrs. into PID (Partial Carbon)	35 Hrs. into PIR (Full Carbon)
				

Table F 3: EL images of the MFG5 DH2 module through various test stages.

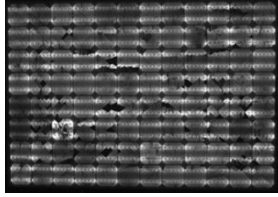
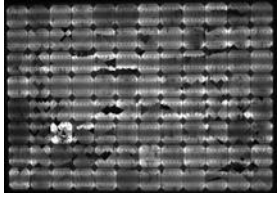
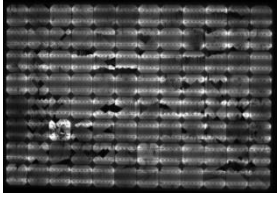
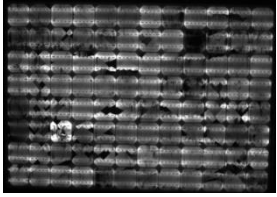
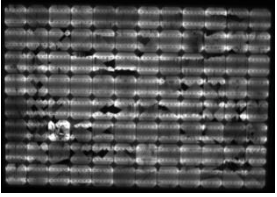
Pre-PID Stressed	5 Hrs. into PID (Partial Carbon)	10 Hrs. into PID (Partial Carbon)	35 Hrs. into PID (Partial Carbon)	35 Hrs. into PIR (Full Carbon)
				

Table F 4: EL images of the MFG5 TC2 module through various test stages.

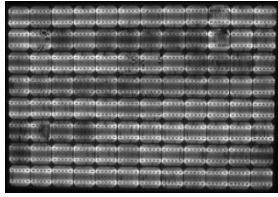
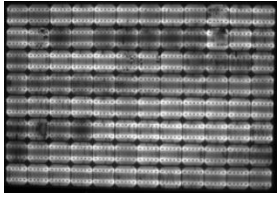
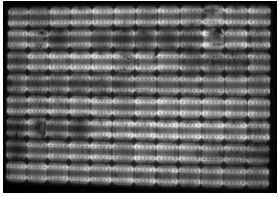
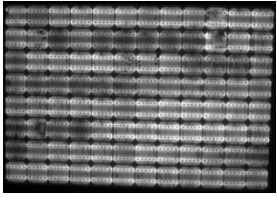
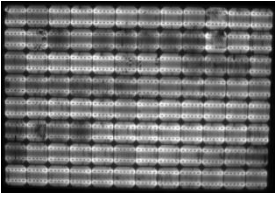
Pre-PID Stressed	5 Hrs. into PID (Partial Carbon)	10 Hrs. into PID (Partial Carbon)	35 Hrs. into PID (Partial Carbon)	35 Hrs. into PIR (Full Carbon)
				

Table F 5: EL images of the MFG6 DH1 module through various test stages.

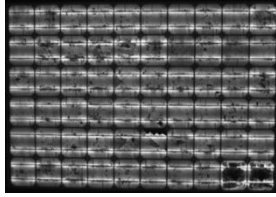
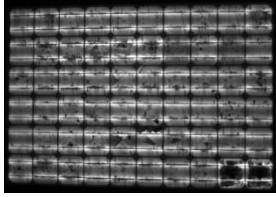
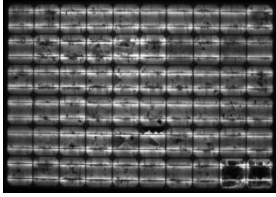
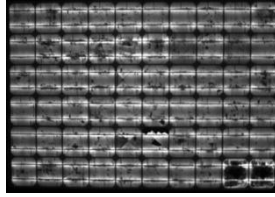
Pre-PID Stressed	5 Hrs. into PID (Partial Carbon)	10 Hrs. into PID (Partial Carbon)	35 Hrs. into PID (Partial Carbon)	35 Hrs. into PIR (Full Carbon)
			NA	

Table F 6: EL images of the MFG6 TC1 module through various test stages.

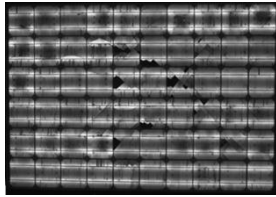
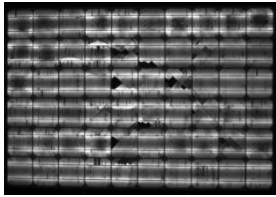
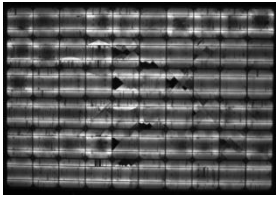
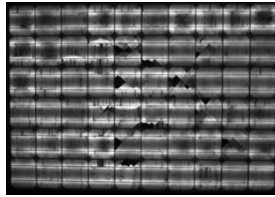
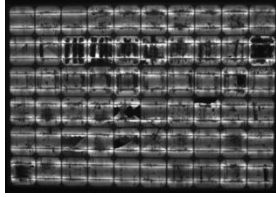
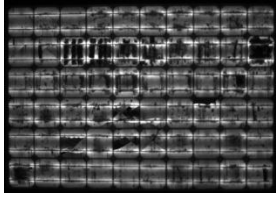
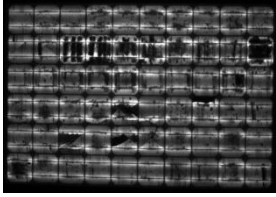
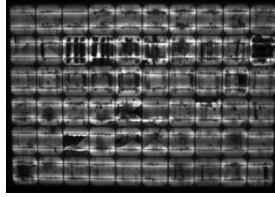
Pre-PID Stressed	5 Hrs. into PID (Partial Carbon)	10 Hrs. into PID (Partial Carbon)	35 Hrs. into PID (Partial Carbon)	35 Hrs. into PIR (Full Carbon)
			NA	

Table F 7: EL images of the MFG6 DH2 module through various test stages.

Pre-PID Stressed	5 Hrs. into PID (Partial Carbon)	10 Hrs. into PID (Partial Carbon)	35 Hrs. into PID (Partial Carbon)	35 Hrs. into PIR (Full Carbon)
			NA	

∞

Table F 8: EL images of the MFG6 TC2 module through various test stages.

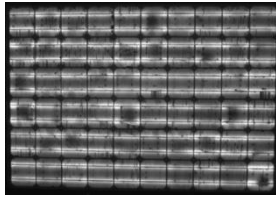
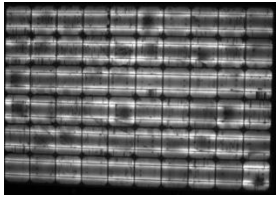
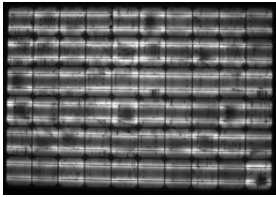
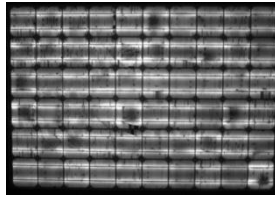
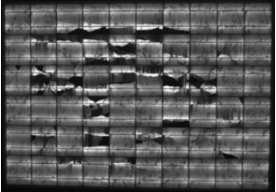
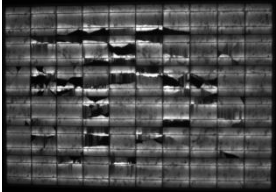
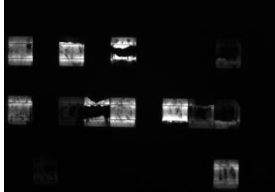
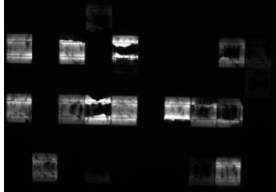
Pre-PID Stressed	5 Hrs. into PID (Partial Carbon)	10 Hrs. into PID (Partial Carbon)	35 Hrs. into PID (Partial Carbon)	35 Hrs. into PIR (Full Carbon)
			NA	

Table F 9: EL images of the MFG7 DH1 module through various test stages.

Pre-PID Stressed	35 Hrs. into PID (Partial Carbon)	35 Hrs. into PID (Full Carbon)	35 Hrs. into PIR (Full Carbon)
			

68

Table F 10: EL images of the MFG7 TC1 module through various test stages.

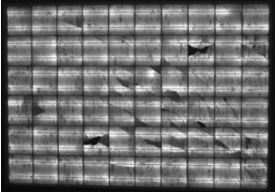
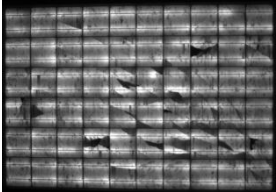
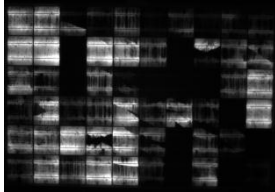
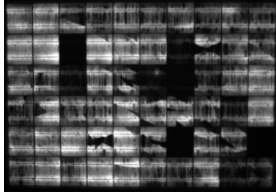
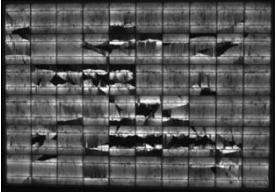
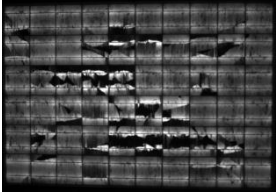
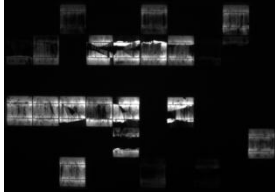
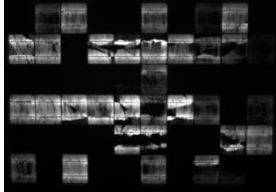
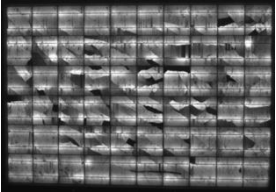
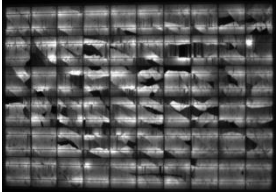
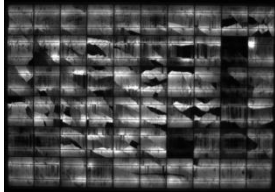
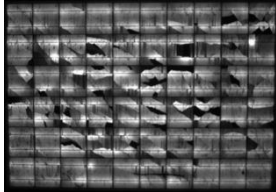
Pre-PID Stressed	35 Hrs. into PID (Partial Carbon)	35 Hrs. into PID (Full Carbon)	35 Hrs. into PIR (Full Carbon)
			

Table F 11: EL images of the MFG7 DH2 module through various test stages.

Pre-PID Stressed	35 Hrs. into PID (Partial Carbon)	35 Hrs. into PID (Full Carbon)	35 Hrs. into PIR (Full Carbon)
			

06

Table F 12: EL images of the MFG7 TC2 module through various test stages.

Pre-PID Stressed	35 Hrs. into PID (Partial Carbon)	35 Hrs. into PID (Full Carbon)	35 Hrs. into PIR (Full Carbon)
			

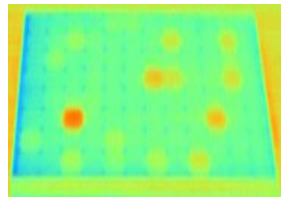
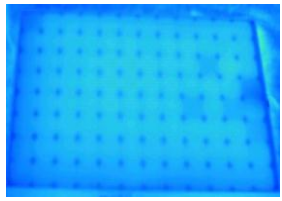
APPENDIX G

[INFRA-RED IMAGING]

DATA COLLECTED AUGUST 2011-APRIL 2012



Table G 1: IR images of MFG5 DH1 module through various test stages.

Before PID	10 Hrs. into PID (Partial Carbon)	35 Hrs. into PID (Partial Carbon)	35 Hrs. into PIR (Full Carbon)
		NA	NA

92

Table G 2: IR images of MFG5 TC1 module through various test stages.

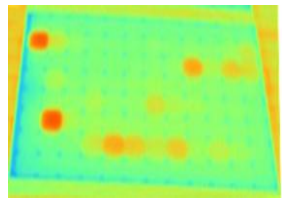
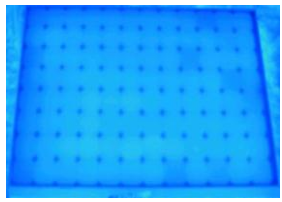
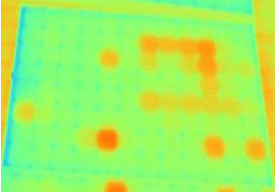
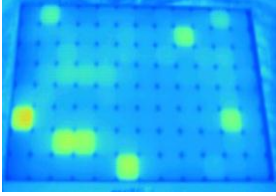
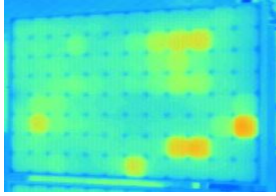
Before PID	10 Hrs. into PID (Partial Carbon)	35 Hrs. into (Partial Carbon)	35 Hrs. into PIR (Full Carbon)
		NA	NA

Table G 3: IR images of MFG5 DH2 module through various test stages.

Before PID	10 Hrs. into PID (Partial Carbon)	35 Hrs. into PID (Partial Carbon)	35 Hrs. into PIR (Full Carbon)
		<p data-bbox="1171 505 1220 537">NA</p>	

93

Table G 4: IR images of MFG5 TC2 module through various test stages.

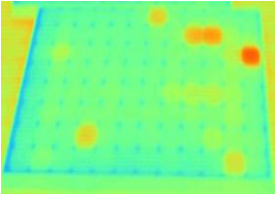
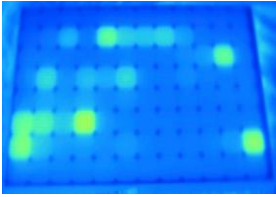
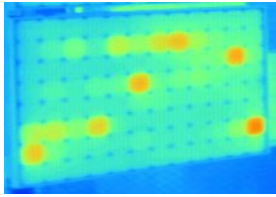
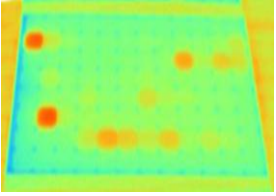
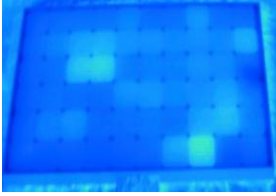
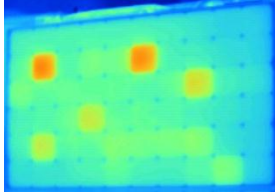
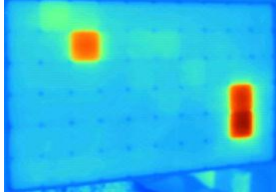
Before PID	10 Hrs. into PID (Partial Carbon)	35 Hrs. into PID (Partial Carbon)	35 Hrs. into PIR (Full Carbon)
			

Table G 5: IR images of MFG6 DH1 module through various test stages.

Before PID	10 Hrs. into PID (Partial Carbon)	35 Hrs. into PID (Partial Carbon)	35 Hrs. into PIR (Full Carbon)
			

94

Table G 6: IR images of MFG6 TC1 module through various test stages.

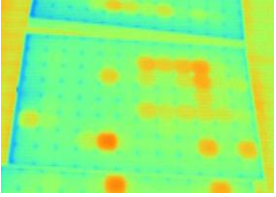

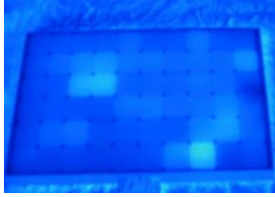
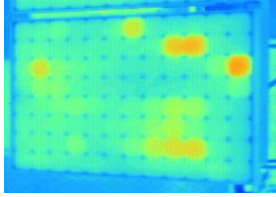
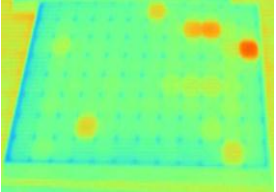
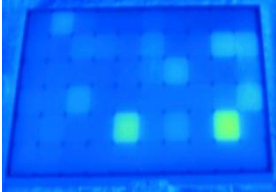
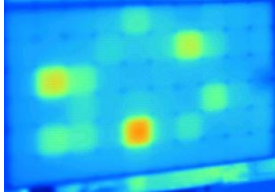
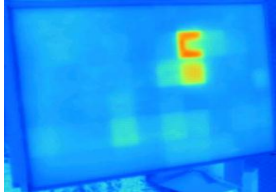
Before PID	10 Hrs. into PID (Partial Carbon)	35 Hrs. into PID (Partial Carbon)	35 Hrs. into PIR (Full Carbon)
			

Table G 7: IR images of MFG6 TC2 module through various test stages.

Before PID	10 Hrs. into PID (Partial Carbon)	35 Hrs. into PID (Partial Carbon)	35 Hrs. into PIR (Full Carbon)
			

95

Table G 8: IR images of MFG6 DH2 module through various test stages.

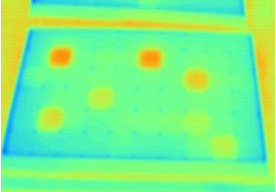
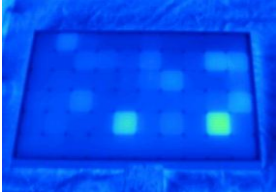
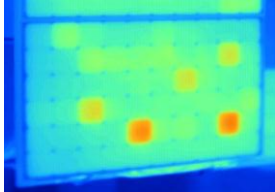
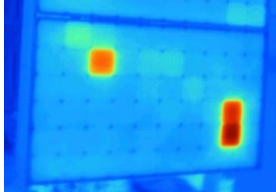
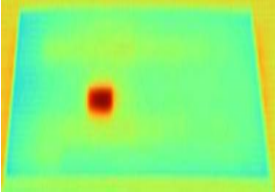


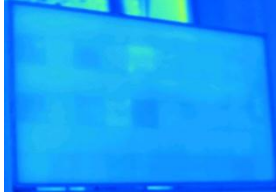
Before PID	10 Hrs. into PID (Partial Carbon)	35 Hrs. into PID (Partial Carbon)	35 Hrs. into PIR (Full Carbon)
			

Table G 9: IR images of MFG7 DH1 module through various test stages.

Pre-PID Stressed	35 Hrs. into PID (Partial Carbon)	35 Hrs. into PID (Full Carbon)	35 Hrs. into PIR (Full Carbon)
			

96

Table G 10: IR images of MFG7 TC1 module through various test stages.

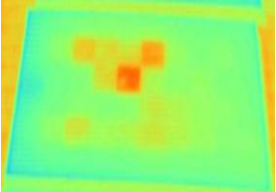
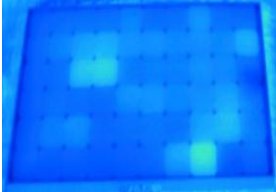
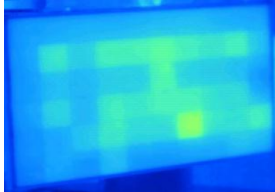

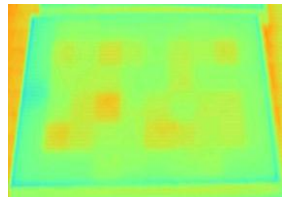
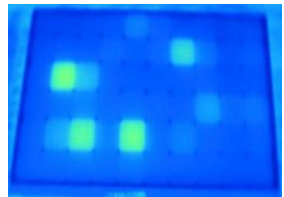
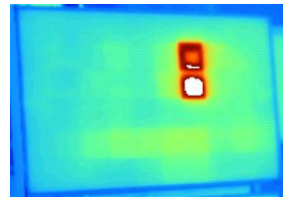
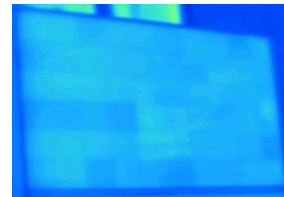
Pre-PID Stressed	35 Hrs. into PID (Partial Carbon)	35 Hrs. into PID (Full Carbon)	35 Hrs. into PIR (Full Carbon)
			

Table G 11: IR images of MFG7 DH2 module through various test stages.

Pre-PID Stressed	35 Hrs. into PID (Partial Carbon)	35 Hrs. into PID (Full Carbon)	35 Hrs. into PIR (Full Carbon)
			

97

Table G 12: IR images of MFG7 TC2 module through various test stages.

Pre-PID Stressed	35 Hrs. into PID (Partial Carbon)	35 Hrs. into PID (Full Carbon)	35 Hrs. into PIR (Full Carbon)
